行政院國家科學委員會補助專題研究計畫成果報告
期末報告

新穎?亞硝醯基鐵化合物之合成、結構、反應性及其電子結構之探討(第 2 年)

計 畫 類 別 ：個別型計畫
計 畫 編 號 ：NSC 100-2113-M-040-004-MY2
執 行 期 間 ：101 年 08 月 01 日至 102 年 12 月 31 日
執 行 單 位 ：中山醫學大學應用化學系（所）

計 畫 主 持 人：陳建宏

計畫參與人員：碩士班研究生-兼任助理人員：蔡孟修
大專生-兼任助理人員：顏詩穎
大專生-兼任助理人員：黃資庭

處 理 方 式 ：
1.公開資訊：本計畫涉及專利或其他智慧財產權，2 年後可公開查詢
2.「本研究」是否已有嚴重損及公共利益之發現：否
3.「本報告」是否建議提供政府單位施政參考：否

中 華 民 國 103 年 02 月 27 日

中 文 摘 要 ： 本計畫成功的合成[O,N]/[S,N]/[NH,N]配位形式的{Fe(NO)2}10 DNICs,並對其化學反應性做出探討.
同時,本計畫亦成功發現單核雙亞硝基鐵化合物及雙核雙亞硝基鐵化合物之間的轉換可藉由其陽離子的不同來調控.

中文關鍵詞： 雙亞硝基鐵化合物

英 文 摘 要 ： The anionic {Fe(NO)2}10 DNICs [K-18-crown-6-ether][(NO)2Fe(NC9H6-NH)] (1), [K-18-crown-6-ether][(NO)2Fe(NC9H6-O)] (2), and [K-18-crown-6-ether][(NO)2Fe(NC9H6-S)] (3) containing [N,NH], [N,O], and [N,S] ligations, respectively, were synthesized via displacing the TMEDA group of {Fe(NO)2}10 (TMEDA)Fe(NO)2 with quinolin-8-amide, quinolin-8-olate, and quinolin-8-thiolate, respectively. The anionic {Fe(NO)2}10 DNICs 1-3 were characterized by IR, UV-vis, and single-crystal X-ray diffraction. The binding affinity of ligands ([NC9H6-NH]－, [NC9H6-O]－, and [NC9H6-S]－) toward the {Fe(NO)2}10 fragment were also investigated and followed the ligand-substitution series [NC9H6-S]－刚 [NC9H6-O]－＞[NC9H6-NH]－. In addition, the displacement of TMEDA group of (TMEDA)Fe(NO)2 by [K-18-crown-6-ether][SC6H4-o-NH2] and [PPh4][SC6H4-o-NH2] afforded mononuclear {Fe(NO)2}10 DNIC [K-18-crown-6-ether][(NO)2Fe(SC6H4-o-NH2)] (4) and dinuclear {Fe(NO)2}10-{Fe(NO)2}10 DNIC [PPh4]2[(NO)2Fe(贡-SC6H4-o-NH2)]2 (5), respectively. Of importance, DNICs 4 and 5 are chemically interconvertible by introducing [PPh4]+ and [K-18-crown-6-ether]+ into the solutions of DNICs 4 and 5, respectively. The observation that the countercation functions to modulate the formation of mononuclear {Fe(NO)2}10 DNIC 4 or dinuclear {Fe(NO)2}10-{Fe(NO)2}10 DNIC 5 was also demonstrated upon reduction of the {Fe(NO)2}9 DNICs [cation][(NO)2Fe(SC6H4-o-NH2)2] (7) (cation = K-18-crown-6-ether (7a), [PPh4] (7b)).

英文關鍵詞： dinitrosyl iron complexes

行政院國家科學委員會補助專題研究計畫成果報告

（□期中進度報告/■期末報告）

新穎雙亞硝醯基鐵化合物之合成、結構、反應性及其電子結構之探討

計畫類別：■個別型計畫　□整合型計畫

計畫編號：NSC 100－2113－M －040－004 －MY2

執行期間： 100 年 08 月 1 日至 102 年 12 月 31 日

執行機構及系所：中山醫學大學 應用化學系

計畫主持人：陳建宏

計畫參與人員：蔡孟修、黃資庭、顏詩穎、張博雅

本計畫除繳交成果報告外，另含下列出國報告，共 _0_ 份：

□執行國際合作與移地研究心得報告

□出席國際學術會議心得報告

期末報告處理方式：

1. 公開方式：
   □非列管計畫亦不具下列情形，立即公開查詢
   ■涉及專利或其他智慧財產權，□一年■二年後可公開查詢
2. 「本研究」是否已有嚴重損及公共利益之發現：■否 □是
3. 「本報告」是否建議提供政府單位施政參考 ■否 □是，（請列舉提供之單位；本會不經審議，依勾選逕予轉送）

中　華　民　國　103 年 2 月 27 日

國科會補助專題研究計畫成果報告自評表

請就研究內容與原計畫相符程度、達成預期目標情況、研究成果之學術或應用價值（簡要敘述成果所代表之意義、價值、影響或進一步發展之可能性）、是否適合在學術期刊發表或申請專利、主要發現（簡要敘述成果是否有嚴重損及公共利益之發現）或其他有關價值等，作一綜合評估。

1. 請就研究內容與原計畫相符程度、達成預期目標情況作一綜合評估

   ■ 達成目標

   □ 未達成目標（請說明，以 100 字為限）

   □ 實驗失敗

   □ 因故實驗中斷

   □ 其他原因

   說明：

2. 研究成果在學術期刊發表或申請專利等情形：

   論文：□已發表 □未發表之文稿 ■ 撰寫中 □無

   專利：□已獲得 □申請中 ■ 無

   技轉：□已技轉 □洽談中 ■ 無

   其他：（以 100 字為限）

3. 請依學術成就、技術創新、社會影響等方面，評估研究成果之學術或應用價值（簡要敘述成果所代表之意義、價值、影響或進一步發展之可能性），如已有嚴重損及公共利益之發現，請簡述可能損及之相關程度（以 500 字為限）

   所合成的新穎化合物,可用以收集其各種光譜數據,應用於探討生物體內一氧化氮與目標物進行反應時,中間各種產物的光譜對照數據。

These results are underprepared to submit.

Introduction

Nitric oxide (NO) is the first gaseous molecule known to act as a signaling molecule[1] and it regulates multiple physiological processes including inflammation, immune system response,[2] neuronal transmission,[3] vasodilatation,[4] and cancer therapy.[5] As a result of the high reactivity of NO, dinitrosyl iron complexes (DNICs) have been recognized as endogenous NO carrier and storage as well as S-nitrosothiols (RSNOs).[6] However, recent study has revealed that DNICs is more favorable for the storage and delivery of NO than the analogous bioorganic RSNOs which were traditionally considered to stabilize the highly reactive NO for transport to various biological process centers, because of the greater stability of DNICs than RSNOs.[7] The naturally occurring DNICs are classified into protein-bound DNICs and low-molecular-weight DNICs (LMW-DNICs). In vivo, protein-bound DNICs derived from NO-mediated degradation of Fe-S cluster containing proteins are considered as the storage of NO or $\{Fe(NO)_2\}$ moiety, and LMW-DNICs yielded via the displacement of protein-bound DNICs with free thiols/thiolates are served probably as the donor of NO or $\{Fe(NO)^2\}$ moiety.[8] Roussin's red esters (RREs), the dimeric form of DNICs, are interconvertible to DNICs and considered to perform the same role as DNICs.[8a, 9] The formation of protein-bound dimeric DNICs were observed upon nitrosylation of the [2Fe-2S] clusters in Rieske –type ToMOC protein[10] and the [4Fe-4S] clusters in WhiB-like proteins.[11] Furthermore, the formation of protein-bound RREs accompanied by protein-bound DNICs (4:1 molar ratio) has been reported upon the treatment of NO with the $[4Fe\text{-}4S]^{2+}$ clusters of FNR, a *hmp* gene transcription regulator, on the basis of UV-vis and EPR spectra.[9b, 12] As has been known, the identity and assignment of both sulfur-ligated protein-bound DNICs and LMW-DNICs are based on their distinctive electron paramagnetic resonance (EPR) signals at g = 2.03 while the characterization of dimeric DNICs in biological system is limited because of its EPR silence.[8d, 13] Despite the major thiol components of cellular DNICs composed of cysteine and glutathione in vivo, cysteinate, histidine, deportonated imidazole, and tyrosinated may also trap the dinitrosyl iron moiety in enzymology based on EPR spectra.[9b, 14] Recently, the single example of a crystallographically characterized protein-bound DNIC, derived from introducing an exogeneously formed $(glutathione)_2Fe(NO)_2$ into human glutathione S-transferase (GST P1-1), has been demonstrated.[14a] Enzyme recognition of the modified glutathione resulted in the binding of $\{Fe(NO)_2\}$ moiety within the active site of these enzyme through the phenolate oxygen of tyrosine of the active site and the sulfur from glutathione that would normally be expected to reside in the active site. Although the

protein-bound DNIC with [S,O] ligation mode was well characterized by X-ray diffraction, it is still difficult for isolation and structural determination of the DNICs derived from NO-mediated biological processes. The difficulty has inspired the efforts in the syntheses of adequate DNICs to serve the spectroscopic references for the intermediates in the NO-mediated biological processes and the study of potential NO delivery systems.

In the search of literature precedent in the area of synthetic DNICs, DNICs can be classified into the paramagnetic, oxidized form DNICs ($\{Fe(NO)_2\}^9$ DNICs) and the diamagnetic, reduced from DNICs ($\{Fe(NO)_2\}^{10}$ DNICs), based on the Enemark-Fetham notation.[15] In contrast to numbers of $\{Fe(NO)_2\}^9$ DNICs containing S/O/N-donor ligands,[7b, 13e, 16] limited $\{Fe(NO)_2\}^{10}$ DNICs are reported and commonly stabilized by CO, PR_3 and N-containing ligands.[16c, 17] Until recently, few $\{Fe(NO)_2\}^{10}$ DNICs bound with S-donor ligands were reported.[18] As a matter of fact, the study of transformations between the oxidized $\{Fe(NO)_2\}^9$ and the reduced $\{Fe(NO)_2\}^{10}$ forms in biology has implicated that the transformations may regulate the role of DNICs for NO storage or as an NO donor.[19] Moreover, in addition to the typically dimeric DNICs with $\{Fe(NO)_2\}^9$-$\{Fe(NO)_2\}^9$ core, the dimeric DNICs containing $\{Fe(NO)_2\}^9$-$\{Fe(NO)_2\}^9$/$\{Fe(NO)_2\}^9$-$\{Fe(NO)_2\}^{10}$ core were prepared and characterized by IR, UV-vis, and single-crystal X-ray diffraction.[18a, 18c, 20] In addition to traditionally four coordinated DNICs, efforts in the syntheses also led to the discovery of several DNICs of higher coordination number.[21]

Based on the study of these reported DNICs, the discrimination of the $\{Fe(NO)_2\}^9$ DNICs with various coordinated ligands (imidazolate, imidazole, amide, thiolate and carboxylate) has been established via the combination of EPR (pattern) and IR ν_{NO} spectra (the separation of NO stretching frequencies).[16f, 22] The interconversion among Roussin's red ester (RRE), anionic $\{Fe(NO)_2\}^9$ DNICs with [S,S]/[S,O]/[S,N]/[N,N] ligation modes, cationic $\{Fe(NO)_2\}^9$ DNICs and neutral $\{Fe(NO)_2\}^{10}$ DNICs with [N,N] coordination mode via protonation, bridged-thioate cleavage reactions triggered by incoming S/N/O-containing ligands, and ligand displacement reactions were demonstrated.[7b, 13e, 16e, 16f] In addition, the facile transformations and relative binding preference of phenolate, thiolate, imidazolate, and nitrite toward the $\{Fe(NO)_2\}^9$ moiety were also studied.[13e] Furthermore, the reversible interconversion with no dissociation of the coordinated ligands of the structurally analogous $\{Fe(NO)_2\}^9$/$\{Fe(NO)_2\}^{10}$ DNICs were also successfully demonstrated.[18a, 18b] Also, it is of importance to note that the EPR spectra of dinuclear $\{Fe(NO)_2\}^9$-$\{Fe(NO)_2\}^{10}$ DNICs which are identical to those of reduction of DNICs/aconitase and HiPIP-containing protein-bound DNIC reveals that the nitrosylation of the $[4Fe\text{-}4S]^{2+}$ clusters of aconitase/HiPIP produces a mixture of the

mononuclear and dinuclear DNICs; namely, anionic RREs as DNICs are another forms in biological system for storage and transport of NO or $\{Fe(NO)_2\}$ moiety.[20] According to the study on the X-ray absorption spectra of these synthetic mononuclear and dinuclear DNICs, probing the formation of EPR-silent $\{Fe(NO)_2\}^9$-$\{Fe(NO)_2\}^9$ and $\{Fe(NO)_2\}^{10}$-$\{Fe(NO)_2\}^{10}$ in biology has been made possible via the Fe K-edge pre-edge energies ;[13e, 18a] in the meantime, unambiguous characterization and discrimination the various oxidation-state dinuclear $\{Fe(NO)_2\}^{9/10}$-$\{Fe(NO)_2\}^{9/10}$ DNICs is also established by the distinct S K-edge pre-edge energy and pattern of these DNICs.[23] In this manuscript, the synthesis, reactivity, and transformation of the anionic $\{Fe(NO)_2\}^{10}$ $[(NO)_2Fe(NC_9H_6\text{-}NH)]^-$ (**1**), $[(NO)_2Fe(NC_9H_6\text{-}O)]^-$ (**2**), and $[(NO)_2Fe(NC_9H_6\text{-}S)]^-$ (**3**), were described. The binding affinity of toward the $\{Fe(NO)_2\}^{10}$ motif was investigated. Additionally, the syntheses and interconversion of anionic $[(NO)_2Fe(SC_6H_4\text{-}o\text{-}NH_2)]^-$ (**4**) and dianionic $\{Fe(NO)_2\}^{10}$-$\{Fe(NO)_2\}^{10}$ $[(NO)_2Fe(\mu\text{-}SC_6H_4\text{-}o\text{-}NH_2)]_2^{2-}$ (**5**) were delineated. Also, the transformations of anionic $\{Fe(NO)_2\}^{10}$ (**4**) and dianionic $\{Fe(NO)_2\}^{10}$-$\{Fe(NO)_2\}^{10}$ (**5**) into anionic $\{Fe(NO)_2\}^9$, anionic $\{Fe(NO)_2\}^{10}$-$\{Fe(NO)_2\}^9$ and neutral $\{Fe(NO)_2\}^9$-$\{Fe(NO)_2\}^9$ DNICs were demonstrated.

Results and Discussion

Syntheses of monomeric $\{Fe(NO)_2\}^{10}$ DNICs containing quinolin-8-amide (1) ($[NC_9H_6\text{-}NH]^-$), quinolin-8-olate (2) ($[NC_9H_6\text{-}O]^-$), quinolin-8-thiolate (3) ($[NC_9H_6\text{-}S]^-$). It has been demonstrated that $\{Fe(NO)_2\}^{10}$ DNICs bound with [S,S] and [N, N] ligations can be easily prepared by displacing the TMEDA group of $(TMEDA)Fe(NO)_2$ precursor with two equiv of thiolates and amides, respectively.[18b] In order to study the properties of $\{Fe(NO)_2\}^{10}$ DNICs with different ligations, a series of $\{Fe(NO)_2\}^{10}$ DNICs containing [N, NH], [N, S] and [N,O] ligations were prepared as shown in Scheme 1a-c. After $(TMEDA)Fe(NO)_2$ and one equiv of [K-18-crown-6-ether][NC_9H_6-NH], [K-18-crown-6-ether][NC_9H_6-O], and [K-18-crown-6-ether][NC_9H_6-S] were stirred, respectively, in THF at ambient temperature under N_2 atmosphere overnight, the substantial amounts of [K-18-crown-6-ether][$(NO)_2Fe(NC_9H_6\text{-}NH)$] (**1**), [K-18-crown-6-ether][$(NO)_2Fe(NC_9H_6\text{-}O)$] (**2**), and [K-18-crown-6-ether][$(NO)_2Fe(NC_9H_6\text{-}S)$] (**3**) were crystallized from THF-hexane as purple crystals of complex **1** in 71.7% yield, yellow-brown crystals of complex **2** in 71.5% yield, and dark-red crystals of complex **3** in 79.9%, respectively, and characterized by IR, UV-vis, ^1H NMR and single-crystal X-ray diffraction. In contrast

to numerous of the anionic $\{Fe(NO)_2\}^9$ DNICs bound with S/N/O-containing lignads, complexes **1**, **2**, and **3** are the rare examples of anionic $\{Fe(NO)_2\}^{10}$ DNICs coordinated by S/N/O-containing lignads, characterized by single-crystal X-ray diffraction. Complexes **1**, **2** and **3** are soluble in THF/CH_3CN and exhibit extremely air sensitivity. The sharp, well-resolved ^1H NMR spectra of complexes **1**, **2** and **3** revealed that complexes **1**, **2** and **3** are diamagnetic as expected for the $\{Fe(NO)_2\}^{10}$ species. The IR spectra for complexes **1**, **2**, and **3** exhibited the same pattern but differed slightly in positions. The IR spectra showing the diagnostic IR ν_{NO} stretching frequencies at 1655 m and 1603 s cm^{-1} (THF) with $\Delta\nu_{NO}$ = 52 cm^{-1} ($\Delta\nu_{NO}$ is the separation of NO stretching frequencies 1655 m and 1603 s cm^{-1}) for complex **1**, at 1674 m, 1619 s cm^{-1} (THF) with $\Delta\nu_{NO}$ = 55 cm^{-1} for complex **2**, at 1660 m, 1612 s (3) cm^{-1} (THF) with $\Delta\nu_{NO}$ = 48 cm^{-1} for complex **3**, are comparable with those of the other anionic $\{Fe(NO)_2\}^{10}$ DNICs.[16c, 18c] The shifts of IR ν_{NO} frequency to the lower wavenumbers for the series of complexes **2**, **3**, and **1** indicates that the electronic donating ability of a given bidentate ligand ($[NC_9H_6\text{-}NH]^-$, $[NC_9H_6\text{-}O]^-$ and $[NC_9H_6\text{-}S]^-$) to the $\{Fe(NO)_2\}^{10}$ motif is on the order of $[NC_9H_6\text{-}NH]^-$ > $[NC_9H_6\text{-}S]^-$ > $[NC_9H_6\text{-}O]^-$.

Scheme 1.

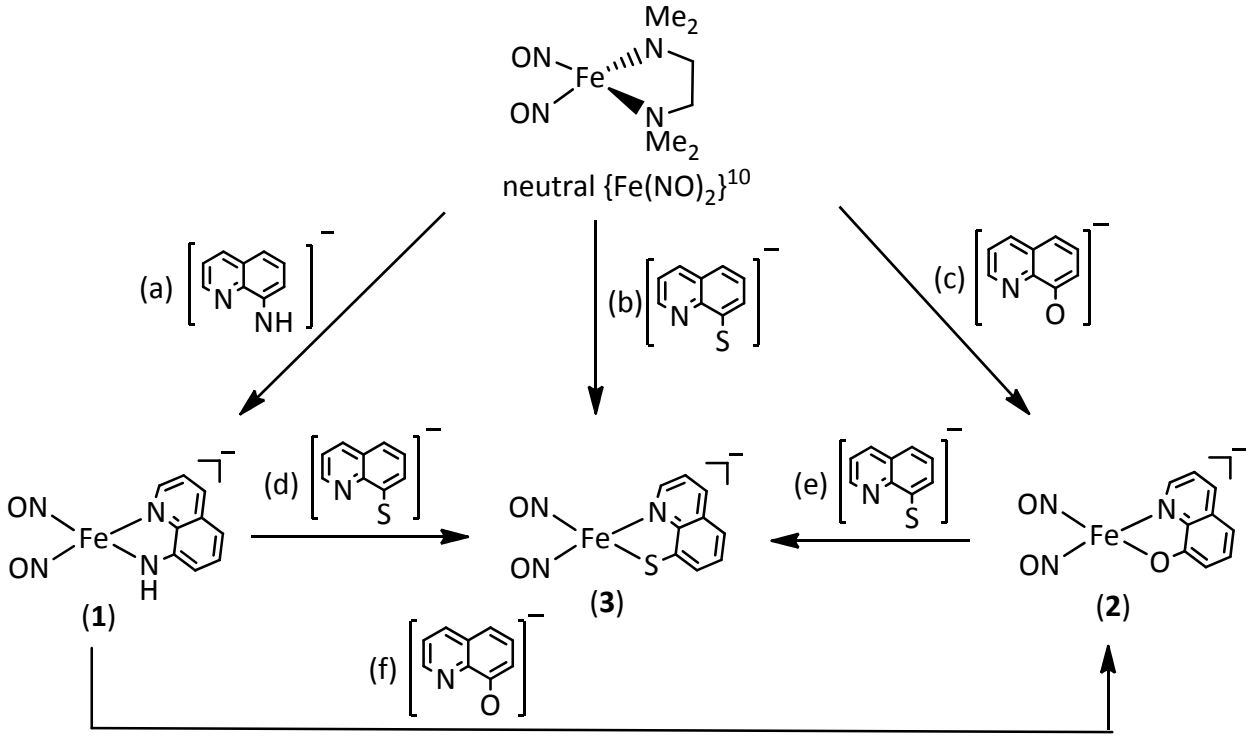

In addition, in order to realize the binding preference of $\{Fe(NO)_2\}^{10}$ motif, the relative binding affinity of the $\{Fe(NO)_2\}^{10}$ motif toward ligands $[NC_9H_6\text{-}NH]^-$, $[NC_9H_6\text{-}O]^-$ and $[NC_9H_6\text{-}S]^-$ was determined by the ligand-exchange reactions

(Scheme 1d-f). Reaction of complex **1** and one equiv of $[NC_9H_6\text{-}O]^-$ and $[NC_9H_6\text{-}S]^-$, respectively, in THF solution at ambient temperature resulted in the shift in IR ν_{NO} from 1655 m, 1603 s cm^{-1} to 1674 m, 1619 s cm^{-1} and 1660 m, 1612 s cm^{-1}, respectively, which were in accordance with the formation of complexes **2** and **3**, respectively (Scheme 1f and 1d). Similarly, the ligand-substitution reaction of complex **2** with one equiv of $[NC_9H_6\text{-}S]^-$ was also conducted. Conversion of complex **2** into complex **3**, monitored by IR ν_{NO} spectroscopy (the shift of the ν_{NO} stretching frequencies from 1674 m, 1619 s cm^{-1} to 1660 m, 1612 s cm^{-1}), was observed when a THF solution of complex **2** was reacted with one equiv of $[NC_9H_6\text{-}S]^-$ at ambient temperature (Scheme 1e). The results of these ligand-displacement reactions concluded that the binding affinity of ligands ($[NC_9H_6\text{-}NH]^-$, $[NC_9H_6\text{-}O]^-$ and $[NC_9H_6\text{-}S]^-$) toward the $\{Fe(NO)_2\}^{10}$ motif is in the order of $[NC_9H_6\text{-}S]^- > [NC_9H_6\text{-}O]^- > [NC_9H_6\text{-}NH]^-$. The trend of binding affinity for these given ligands toward the $\{Fe(NO)_2\}^{10}$ motif is not consistent with the previous result that the $\{Fe(NO)_2\}^{10}$ moiety shows a stronger binding affinity toward the weaker electron-donating ligands while the $\{Fe(NO)_2\}^{9}$ motif shows a more favorable binding preference for the stronger electron-donating ligands over the weaker electron-donating ligands.[18b] Presumably, the conversions of complexes **1** and **2** to complex **3** is ascribed that the stronger interaction between the soft thiolate ligand and the electron rich $\{Fe(NO)_2\}^{10}$ motif (soft-soft interaction) dominates over the electronic effect of ligands toward $\{Fe(NO)_2\}^{10}$ motif. Combination of the studies on the binding affinity for the S/N/O containing lignads toward $\{Fe(NO)_2\}^{10}$ and $\{Fe(NO)_2\}^{9}$ moieties may imply that both of the nature occurring protein-bound $\{Fe(NO)_2\}^{10}$ and $\{Fe(NO)_2\}^{9}$ DNICs prefer binding to the proteins through the thiolate groups of cysteinate/glutathione side chains in the biological systems.

Synthesis and Reactivity of dimeric $\{Fe(NO)_2\}^{10}$ DNIC. In a similar fashion, synthesis of another anionic monomer $\{Fe(NO)_2\}^{10}$ DNIC bound with [N,S] ligation by reaction of $(TMEDA)Fe(NO)_2$ and one equiv of [K-18-crown-6-ether][SC_6H_4-*o*-NH_2] was investigated in CH_3CN under the nitrogen atmosphere at ambient temperature. The shift in IR ν_{NO} from 1690 m, 1634 s cm^{-1} to 1657 m, 1607 s cm^{-1} (CH_3CN) is in accordance with the formation of the monomeric $\{Fe(NO)_2\}^{10}$ [K-18-crown-6-ether][$(NO)_2Fe(SC_6H_4$-*o*-$NH_2)$] (**4**), which was characterized by IR, UV-vis, ^1H NMR, and single-crystal X-ray diffraction (Scheme 2a). In contrast to the reaction of $(TMEDA)Fe(NO)_2$ with [K-18-crown-6-ether][SC_6H_4-*o*-NH_2] yielding the monomeric complex **4**, the treatment of $(TMEDA)Fe(NO)_2$ and [PPh_4][SC_6H_4-*o*-NH_2] in 1:1 stoichiometry in CH_3CN led to the formation of dimeric $[PPh_4]_2[(NO)_2Fe(\mu\text{-}SC_6H_4\text{-}o\text{-}NH_2)]_2$ (**5**) (Scheme 2b) which was isolated as thermally stable, crystalline solids, and identified

by IR, UV-vis, ^{1}H NMR, and single-crystal X-ray diffraction. Up to now, only one example of the dianionic reduced RRE containing two $\{Fe(NO)_2\}^{10}$ motifs bridged by thiolates has been reported.[18a] Complex **5** is soluble in the solution of THF-DMSO (1:1 volume ratio) and exhibits extremely air-sensitive in solution but is stable to air for minutes in the solid state. The IR spectrum of complex **5** displays the diagnostic IR ν_{NO} stretching frequencies at 1650 m, 1598 s cm^{-1} (THF: DMSO = 1:1 (v/v)) with $\Delta\nu_{NO}$ = 52 cm^{-1}), consistent with the IR ν_{NO} stretching frequencies of the other dimeric $\{Fe(NO)_2\}^{10}$-$\{Fe(NO)_2\}^{10}$ species.[18a] Based on the sharp, well resolved ^{1}H NMR spectrum, the absence of EPR signal and paramagnetism, complex **5** is best described as a dianionic reduced RRE with a diamagnetic $\{Fe(NO)_2\}^{10}$-$\{Fe(NO)_2\}^{10}$ core. Compared to the Fe K-edge pre-edge energy of 7113.2 eV for $[PPN]_2[(NO)_2Fe(\mu\text{-}S^tBu)]_2$, complex **5** shows the slightly higher pre-edge energy at 7113.3 eV (Figure 1). The relatively weaker electron-donating $[SC_6H_4\text{-}o\text{-}NH_2]^-$ inducing the relatively electron deficient $\{Fe(NO)_2\}^{10}$-$\{Fe(NO)_2\}^{10}$ core of complex **5**, compared to that of $[PPN]_2[(NO)_2Fe(\mu\text{-}S^tBu)]_2$, may rationalize the slightly higher pre-edge energy for complex **5**. Interestingly, we also noted that complexes **4** and **5** were interconvertible via exchanging the cations of complexes **4** and **5**, respectively, as presented in Scheme 2c and 2c'. Upon the addition of $[PPh_4][Br]$ into a CH_3CN solution of complex **4** in 1:1 stoichiometry overnight, the transformation from complex **4** to complex **5** was demonstrated by the formation of the dark green crystals of complex **5**, identified by two characteristic stretching bands at 1647 s, 1606 s cm^{-1} (KBr) of IR spectrum. Reversibly, conversion of complex **5** to complex **4** was displayed when CH_3CN-THF solution (1:1 volume ratio) of $[K][BPh_4]$ and 18-crown-6-ether were stirred with complex **5** at ambient temperature overnight. After recrystallizing the reaction product, the characteristic IR ν_{NO} stretching frequencies at 1645 s, 1605 s cm^{-1} (CH_3CN) was in accordance with the formation of complex 5. It seems that the intermolecular $[Fe(SR)\cdots(K^+)]$ interaction of complex **4**, verified by single-crystal X-ray diffraction in the solid state, triggers the interconversion between complexes **4** and **5**. Presumably, the intermolecular $[Fe(SR)\cdots(K^+)]$ interaction of complex **4** diminished the donation of electron density from the bidentated $[SC_6H_4\text{-}o\text{-}NH_2]^-$ to the Fe center and stabilized the monomeric $\{Fe(NO)_2\}^{10}$ complex **4**. Reversely, the displacement of [K-18-crown-6-ether] with $[PPh_4]$ quenched the intermolecular $[Fe(SR)\cdots(K^+)]$ interaction of complex **4**; meanwhile, the resulting relatively more donation of electron density from the bidentated $[SC_6H_4\text{-}o\text{-}NH_2]^-$ to the Fe center induced the liberation of N atom of $[SC_6H_4\text{-}o\text{-}NH_2]^-$ from Fe center and subsequently dimerized to yield complex **5**. The interconversion between complexes **4** and **5** implicates that the [Fe(Cys)···(cation)]/ [Fe(Cys)···(H)] interaction existing between

the surrounding environment and the monomeric/dimeric $\{Fe(NO)_2\}^{10}$ DNICs may regulate the interconversion between the dimeric $\{Fe(NO)_2\}^{10}$ DNICs with bridging cysteinates and the monomeric $\{Fe(NO)_2\}^{10}$ DNICs coordinated with the S and N atoms of cysteinate in biological system.

Scheme 2.

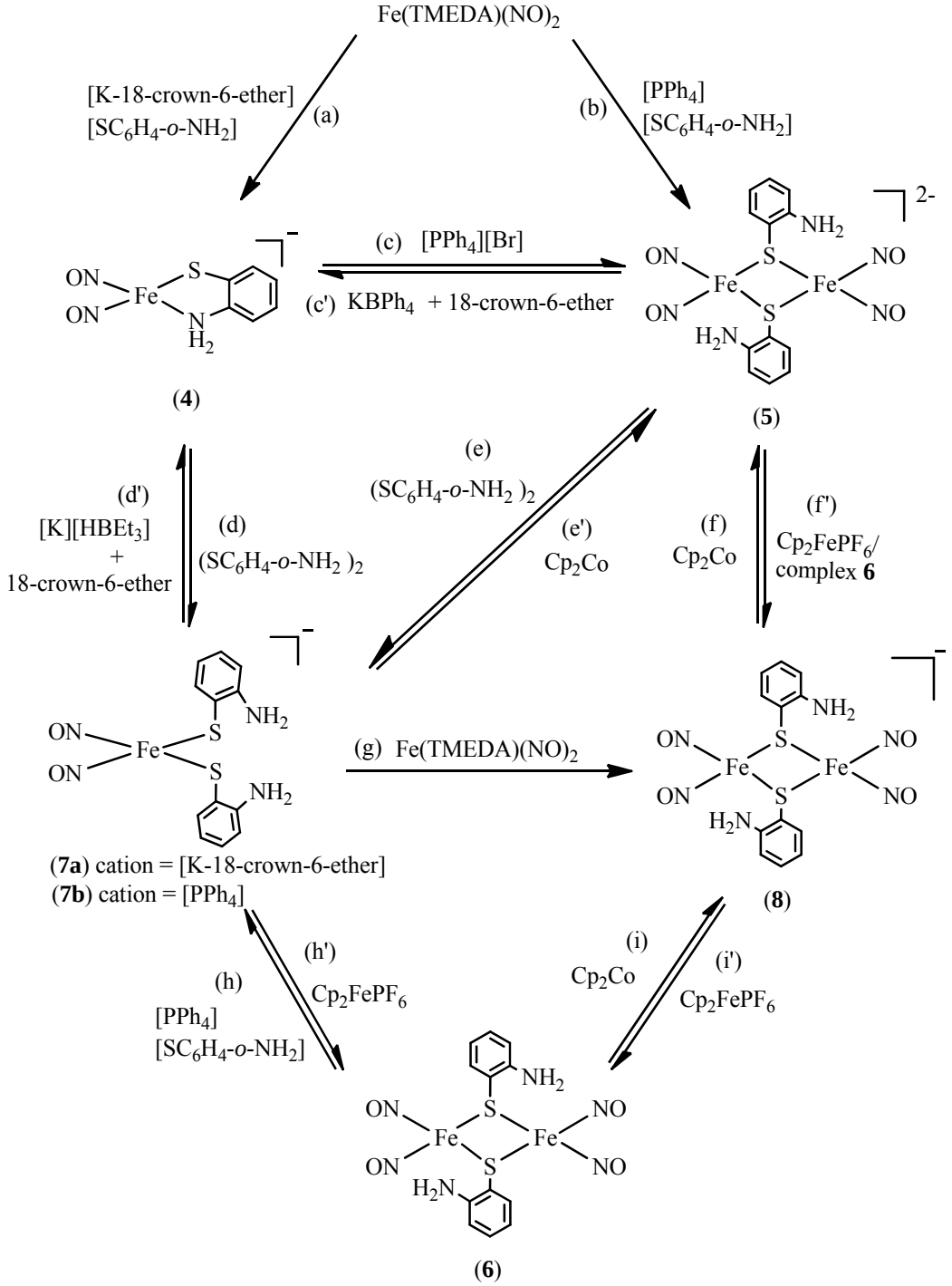

The transformations of the monomeric and dimeric $\{Fe(NO)_2\}^{10}$ DNICs into monomeric $\{Fe(NO)_2\}^{9}$ DNICs were demonstrated as shown in Scheme 2d and 2e by the reactions of complexes **4** and **5** with 1 equiv of $(SC_6H_4\text{-}o\text{-}NH_2)_2$, respectively,

in THF at ambient temperature and monitored by IR ν_{NO} spectroscopy. The IR ν_{NO} stretching frequencies at 1739 s, 1694 s cm^{-1} (THF) indicated the formation of $[(NO)_2Fe(SC_6H_4\text{-}o\text{-}NH_2)_2]^-$ (**7**) (cation = K-18-crown-6-ether (**7a**), $[PPh_4]$ (**7b**)) via oxidation addition of $(SC_6H_4\text{-}o\text{-}NH_2)_2$ into the $\{Fe(NO)_2\}^{10}$ core of complexes **4** and **5**, respectively. Reversibly, chemical reduction of complexes **7a** and **7b** were demonstrated (Scheme 2d' and 2e') and monitored by IR ν_{NO} spectroscopy. Reduction of complex **7a** with $KHBEt_3$ in the presence of 18-crown-6-ether and reduction of complex **7b** with excess Cp_2Co resulted in the yellow-brown solids and green precipitates, respectively. The IR spectra of the yellow-brown solids and green precipitates showed the ν_{NO} stretching frequencies at 1643 m, 1585 s and 1648 s, 1606 s cm^{-1}(KBr), respectively, consistent with the formation of complexes **4** and **5**. Obviously, chemical reduction the $\{Fe(NO)_2\}^9$ core in complex **7** to the electron rich $\{Fe(NO)_2\}^{10}$ motif led to the liberation of one $[SC_6H_4\text{-}o\text{-}NH_2]^-$ from the Fe center and formation the monomeric complex **4** and dimeric complex **5**, respectively, depended on the choice of the distinct cations.

As presented in Scheme 2f', when complex **5** reacted with $[Cp_2Fe][PF_6]$ in 1:1 stoichiometry at ambient temperature under inert atmosphere, transformation of complex **5** into $[PPh_4][(NO)_2Fe(\mu\text{-}SC_6H_4\text{-}o\text{-}NH_2)]_2$ (**8**) was observed and identified by IR, Uv-vis, EPR spectroscopy and single-crystal X-ray diffraction. The characteristic IR ν_{NO} stretching frequencies at 1687 s, 1666 s cm^{-1} (THF) was consistent with the formation of $\{Fe(NO)_2\}^9$-$\{Fe(NO)_2\}^{10}$ complex **8** via one-electron oxidization of the $\{Fe(NO)_2\}^{10}$-$\{Fe(NO)_2\}^{10}$ complex **5**. Alternatively, serving the $\{Fe(NO)_2\}^9$ complex **7** as the chelating metallo-ligand to displace the TMEDA group of the $\{Fe(NO)_2\}^{10}$ $(TMEDA)Fe(NO)_2$ also afforded the $\{Fe(NO)_2\}^9$-$\{Fe(NO)_2\}^{10}$ complex **8** (Scheme 2g). Complex **8** displays an isotropic EPR signal at g = 2.001 at 298 K (Figure S1 in the supporting information (SI)), which is consistent with the other $[(NO)_2Fe(SR)]_2^-$ species whose isotropic g values fall in the range of 1.998-2.004.[17d, 20] Cyclic voltammogram of complex **8** has been recorded in CH_3CN solution containing 0.1 M $[N(n\text{-}Bu)_4][PF_6]$ as supporting electrolyte by a glassy carbon working electrode and a $Ag/AgNO_3$ reference electrode at room temperature (scan rate 0.1 V/s). Remarkably, the cyclic voltammogram of complex **8** reveals two reversible oxidation-reduction processes at -0.82 and -1.24 V ($E_{1/2}$ vs Fc^+/Fc) (Figure S2 in the SI). The redox potential at -0.82 V is assigned for the $\{Fe(NO)_2\}^9$-$\{Fe(NO)_2\}^9$/$\{Fe(NO)_2\}^9$-$\{Fe(NO)_2\}^{10}$ couple corresponding to chemical oxidation of complex **8** as shown in scheme 2i'; meanwhile, the redox potential at -1.24 V is assigned for the $\{Fe(NO)_2\}^9$-$\{Fe(NO)_2\}^{10}$/$\{Fe(NO)_2\}^{10}$-$\{Fe(NO)_2\}^{10}$ couple corresponding to the chemical reduction of complex **8** as shown in 2f. The oxidation of complex **8** was demonstrated by reaction of complex **8** with $[Cp_2Fe][PF_6]$

in a 1:1 stoichiometry at ambient temperature (Scheme 2i'). The IR spectrum displaying the NO stretching frequencies at 1807 w, 1778 s, 1751 s cm^{-1} (THF) was consistent with the formation of $\{Fe(NO)_2\}^9$-$\{Fe(NO)_2\}^9$ complex **6**. Reversibly, reduction of complex **6** into $[(NO)_2Fe(\mu\text{-}SC_6H_4\text{-}o\text{-}NH_2)]_2^-$ under the presence of Cp_2Co was displayed and monitored by IR spectra. The formation of $[Cp_2Co][(NO)_2Fe(\mu\text{-}SC_6H_4\text{-}o\text{-}NH_2)]_2$ was confirmed by the IR ν_{NO} stretching bands at 1686 s, 1665 s cm^{-1} (DMSO: THF = 1:1 (v/v)) (Scheme 2i). The further reduction of $[(NO)_2Fe(\mu\text{-}SC_6H_4\text{-}o\text{-}NH_2)]_2^-$ into $[(NO)_2Fe(\mu\text{-}SC_6H_4\text{-}o\text{-}NH_2)]_2^{2-}$ was also observed upon the addition of excess Cp_2Co to the solution of $[Cp_2Co][(NO)_2Fe(\mu\text{-}SC_6H_4\text{-}o\text{-}NH_2)]_2$ (DMSO: THF = 1:1 (v/v) at ambient temperature. The shift of NO stretching frequencies from 1686 s, 1665 s cm^{-1} to 1650 s, 1598 s (DMSO: THF = 1:1 (v/v) was assigned to the formation of $[Cp_2Co]_2[(NO)_2Fe(\mu\text{-}SC_6H_4\text{-}o\text{-}NH_2)]_2$ (Scheme 2f). We also noted that the intermolecule electron transfer occurred between $\{Fe(NO)_2\}^9$-$\{Fe(NO)_2\}^9$ complex **6** and $\{Fe(NO)_2\}^{10}$-$\{Fe(NO)_2\}^{10}$ complex **5**. As shown in Scheme 2f', reaction of complex **6** with complex **5** in THF at ambient temperature overnight resulted in two strong absorption bands at 1687 s, 1666 s cm^{-1} which was consistent with the formation of complex **8.** Obviously, complexes **5**, **6** and **8** are chemically convertible via redox processes as displayed in Scheme 2f-2f' and 2i-2i' and the interconversion among complexes **5**, **6** and **8** also implicated that in addition to the role for the storage and transfer of NO, DNICs also probably serve as the role for the storage and transport of electrons. Schemes 2h and 2h' demonstrated the reversible interconversion between monomeric $\{Fe(NO)_2\}^9$ complex **7** and dimeric $\{Fe(NO)_2\}^9$-$\{Fe(NO)_2\}^9$ complex **6** via oxidation of complex 7 with Cp_2FePF_6 and bridged-thiolate cleavage of complex **6** with two equiv of thiolates, which has been known in the previous reports.[24]

Structures. Figures 2–5 display the thermal ellipsoid plots of complexes **1**–**4**, respectively, and the selected bond distances and angles are given in the figure captions. The strain effect of the chelating ligands in the coordination sphere of complexes **1**–**4** accounts for the distorted tetrahedral geometry of Fe with N(3)–Fe(1)–N(4) bond angle of 77.2(6)° for complex **1**, N(3)–Fe(1)–O(3) bond angle of 79.1(3)° for complex **2**, N(3)–Fe–S(1) bond angle of 83.11(7)° for complex **3**, and N(3)–Fe(1)–S(1) bond angles of 84.27° for complex **4**, respectively. The observations of complexes **1**–**4** that N(NO)–M–N(NO) bond angles are less than 120° and two oxygen atoms bend toward each other (complex **1**: ∠N(1)–Fe(1)–N(2) 113.2(5)° > ∠O(1)–Fe(1)–O(2) 104.3(3)°; complex **2**: ∠N(1)–Fe(1)–N(2) 114.4(4)° > ∠O(1)–Fe(1)–O(2) 105.6(2)°; complex **3**: ∠N(1)–Fe–N(2) 117.56(12)° > ∠O(1)–Fe–O(2) 109.48(7)°; complex **4**: ∠N(1)–Fe(1)–N(2) 116.2(3)° >

∠O(1)–Fe(1)–O(2) 106.6(2)°) indicates that the iron-dinitrosyl groups of complexes **1**–**4** are considered as "attracto" conformations. The observations are consistent with the suggestion that the "attracto" conformations are generally favored in the first-low transition-metal complexes bound with good π-acceptor ligands.[25] The Fe(1)–N(3) distance of 2.045(7) Å in complex **2** is comparable to the average Fe–N distances of 2.046(4) Å in $Fe(NO)_2(1\text{-MeIm})_2$[17e] and $Fe(NO)_2(bipy)$[17d]; meanwhile, Fe(1)–N(4) distance of 2.053(15) Å in complex **1**, Fe–N(3) distance of 2.067(2) Å in complex **3** and Fe(1)–N(3) distance of 2.085(5) Å in complex **4** are longer than the average Fe–N distances of 2.046(4) Å in $Fe(NO)_2(1\text{-MeIm})_2$ and $Fe(NO)_2(bipy)$. The average $Fe–N_{(NO)}$ bond distances of 1.652(3) Å and 1.647(6) Å in complexes **3** and **4**, respectively, are comparable to those reported in $Fe(NO)_2(1\text{-MeIm})_2$ (average value: 1.649(3) Å) and $Fe(NO)_2(bipy)$ (average value: 1.650(4) Å), but the average $Fe–N_{(NO)}$ bond distances of 1.622(10) Å and 1.620(11) Å in complexes **1** and **2**, respectively, are clearly shorter than those found in $Fe(NO)_2(1\text{-MeIm})_2$ and $Fe(NO)_2(bipy)$. The average N-O bond lengths of 1.209(3) Å and 1.200(7) Å in complexes **3** and **4**, respectively, exactly fall in the range of 1.214(6)－1.189(4) Å observed in neutral $\{Fe(NO)_2\}^{10}$ DNICs and meanwhile, the average N–O bond lengths of 1.183(13) Å in complex **1** and that of 1.230(13) Å in complex **2** are nearly at the lower and upper end of 1.214(6)－1.189(4) Å, respectively, for the neutral $\{Fe(NO)_2\}^{10}$ DNICs.[16e]

The single-crystal X-ray structures of complexes **5** and **8** are depicted in Figures 6 and 7, and selected bond dimensions are presented in the figure captions. Complex **5** possesses crystallographically imposed centrosymmetry. Two nitrosyl groups and bridging thiolates define the distorted tetrahedral geometry of each iron atom, leading to acute angle Fe－S(1)－Fe(A) 99.76(6)° and S(1)－Fe(1)－S(1A) 80.24(6)°. Compared to $[PPN]_2[(NO)_2Fe(\mu\text{-}S^tBu)]_2$ displaying the butterfly-like structure of the $[Fe(S)_2Fe]$ core,[18a] the geometry of the $[Fe(\mu\text{-}S)_2Fe]$ core in complex **5** is best described as a planar rhombus with two 2-aminophenyl groups adopting an *anti* configuration in the solid. In contrast, the geometry of the $[Fe(\mu\text{-}S)_2Fe]$ core in complex **8** is best described as a slightly butterfly-like structure with a dihedral angle of 175.86° (the intersection of two Fe_2S planes) in the solid state. The apparently longer Fe···Fe(A) distance (3.6408(15) Å) of complex **5** and Fe(1)···Fe(2) distance (2.9258(5) Å) of complex **8**, compared to that of 2.7065(14) Å in complex $[(NO)_2Fe(\mu\text{-}SC_6H_4\text{-}o\text{-}NH_2)]_2$ (**6**) (Figure S3 in the SI), reveal the absence and weaker Fe···Fe interaction in complexes **5** and **8**, respectively. Meanwhile, the mean bridging Fe–S bond distances of 2.3805(18) Å and 2.3128(7) Å observed in complexes **5** and **8**, respectively, are longer than that of 2.2729(15) Å found in complex **6**. The longer mean bridging Fe–S and Fe···Fe distances found in complexes **5** and **8**, respectively, indicate that transformation of $\{Fe(NO)_2\}^9$–$\{Fe(NO)_2\}^9$ complex **6** to

$\{Fe(NO)_2\}^9$–$\{Fe(NO)_2\}^{10}$ complex **8** and $\{Fe(NO)_2\}^{10}$–$\{Fe(NO)_2\}^{10}$ complex **5** results in the elongation of bridging Fe–S distances and the relief of Fe···Fe interaction. The shorter Fe–N bond distances of 1.664(5) Å and 1.662(2) Å and the longer N−O bond distances of 1.186(7) Å and 1.182(3) Å observed in complexes **5** and **8**, respectively, compared to the Fe–N bond distance of 1.673(5) Å and the N−O bond distance of 1.160(6) Å found in complex **6**, are consistent with the better metal π-back-donation to the NO antibonding orbital in complexes **5** and **8**.

Conclusion and Comments

Studies on the monomeric dinitrosyl iron complexes **1**-**4** and dimeric dinitrosyl iron complex **5** have resulted in the following results:

(1) The mononuclaer $\{Fe(NO)_2\}^{10}$ DNICs containing quinolin-8-amide (**1**) ($[NC_9H_6\text{-}NH]^-$), quinolin-8-olate (**2**) ($[NC_9H_6\text{-}O]^-$), quinolin-8-thiolate (**3**) ($[NC_9H_6\text{-}S]^-$) were synthesized successfully. The study on the binding preference of $\{Fe(NO)_2\}^{10}$ moiety for quinolin-8-amide, quinolin-8-olate, quinolin-8-thiolate via the ligand-substitution reaction demonstrated that the binding affinity of these lignads toward $\{Fe(NO)_2\}^{10}$ motifs, respectively, was in the order of $[NC_9H_6\text{-}S]^- > [NC_9H_6\text{-}O]^- > [NC_9H_6\text{-}NH]^-$. The preferred formation of thermally stable thiolate-containing $\{Fe(NO)_2\}^{10}$ DNICs may be depicted as that the predominance of interaction between the softer donor and softer $\{Fe(NO)_2\}^{10}$ motif overwhelmed the favorable interaction between the weaker electron-donating ligand and electron rich $\{Fe(NO)_2\}^{10}$ motif. This result in combination of the previously similar study on $\{Fe(NO)_2\}^9$ moiety reveals that the protein-bound DNICs found in biological systems would show much favor to bind $\{Fe(NO)_2\}^9/\{Fe(NO)_2\}^{10}$ motifs through the thiolate groups of cysteinate/glutathione side chains.

(2) The chemical interconversions among the $\{Fe(NO)_2\}^{10}$ $[(NO)_2Fe(SC_6H_4\text{-}o\text{-}NH_2)]^-$ (**4**), $\{Fe(NO)_2\}^{10}$-$\{Fe(NO)_2\}^{10}$ $[(NO)_2Fe(\mu\text{-}SC_6H_4\text{-}o\text{-}NH_2)]_2^{2-}$ (**5**), $\{Fe(NO)_2\}^{10}$-$\{Fe(NO)_2\}^9$ $[(NO)_2Fe(\mu\text{-}SC_6H_4\text{-}o\text{-}NH_2)]_2^-$ (**8**), $\{Fe(NO)_2\}^9$-$\{Fe(NO)_2\}^9$ $[(NO)_2Fe(\mu\text{-}SC_6H_4\text{-}o\text{-}NH_2)]_2$ (**6**), and $\{Fe(NO)_2\}^9$ $[(NO)_2Fe(SC_6H_4\text{-}o\text{-}NH_2)_2]^-$ (**7**) are demonstrated. The isolation of the homologous dinuclear DNIC redox partners ($[(NO)_2Fe(\mu\text{-}SC_6H_4\text{-}o\text{-}NH_2)]_2^{2-}$, $[(NO)_2Fe(\mu\text{-}SC_6H_4\text{-}o\text{-}NH_2)]_2^-$, and $[(NO)_2Fe(\mu\text{-}SC_6H_4\text{-}o\text{-}NH_2)]_2$) may imply the possibility of DNICs serving as the storage of electrons, such as Fe-S cluster in bioprocesses.

(3) Chemical reduction of $\{Fe(NO)_2\}^9$ $[(NO)_2Fe(SC_6H_4\text{-}o\text{-}NH_2)_2]^-$ (**7a**)/(**7b**) by [K-18-crown-6ether][$HBEt_3$] and $CoCp_2$ affording $[(NO)_2Fe(SC_6H_4\text{-}o\text{-}NH_2)]^-$ (**4**) and $[(NO)_2Fe(\mu\text{-}SC_6H_4\text{-}o\text{-}NH_2)]_2^{2-}$ (**5**), respectively, revealed that the intermolecular $[Fe(SR)\cdots(K^+)]$ interaction, verified by single-crystal X-ray

diffraction study, may modulate the formation of mononuclear $\{Fe(NO)_2\}^{10}$ (**4**) and dinuclear $\{Fe(NO)_2\}^{10}$-$\{Fe(NO)_2\}^{10}$ (**5**). The crucial role of the intermolecular [Fe(SR)···(K^+)] interaction in regulation the existence of mononuclear $\{Fe(NO)_2\}^{10}$ (**4**) or dinuclear $\{Fe(NO)_2\}^{10}$-$\{Fe(NO)_2\}^{10}$ (**5**) is also verified by the interconversion of complexes **4** and **5** via introducing the different counter cations.

We expect that syntheses of the anionic $\{Fe(NO)_2\}^{10}$ complexes **1**-**4** may support/unravel the presence of the protein-bound $\{Fe(NO)_2\}^{10}$ DNICs with [N,N]/[N,S]/[N,O] ligations in the biological system. The reversible conversion from complex **4** to complex **5,** induced by the choice of cations, may provide the opportunity to demonstrate that the [Fe(Cys)···(cation)]/[Fe(Cys)···(H)] interaction between the surrounding environment and the protein-bound monomeric/dimeric $\{Fe(NO)_2\}^{10}$ DNICs modulates the possible binding modes of $\{Fe(NO)_2\}$ fragment in cysteine-containing biomolecules.

Experimental Section

Manipulations, reactions, and transfers were conducted under nitrogen according to Schlenk techniques or in a glovebox (nitrogen gas). Solvents were distilled under nitrogen from appropriate drying agents (methylene chloride from CaH_2; acetonitrile from CaH_2-P_2O_5; diethyl ether, hexane and tetrahydrofuran (THF) from sodium benzophenone) and stored in dried, N_2-filled flasks over 4Å molecular sieves. Nitrogen was purged through these solvents before use. Solvent was transferred to the reaction vessel via stainless cannula under positive pressure of N_2. The reagents tetraphenylphosphonium bromide ([PPh_4][Br]), iron pentacarbonyl (Strem), 18-crown-6-ether, (Aldrich-Sigma), *N*,*N*,*N*′,*N*′-Tetramethylethylenediamine (TMEDA), nitrosonium tetrafluoroborate (Alfa Aesar), 8-aminoquinoline, 8-quinolinol (TCI), 8,8'-dithiodiquinoline and 2-aminothiophenol (Acros) were used as received. [PPN][$Fe(CO)_3(NO)$], and (TMEDA)$Fe(NO)_2$ have been prepared according to the literature procedure.[16e, 26] Infrared spectra of the carbonyl ν(CO) and the nitrosyl ν(NO) stretching frequencies were recorded on Bruker ALPHA FT-IR spectrophotometer and Thermo FT-IR Nicolet iS5/iD1 spectrophotometer with sealed solution cells (0.1 mm, KBr/CaF_2 windows) or KBr disc. UV/vis spectra were recorded on a Thermo Evolution 201 UV-Visible spectrophotometer. Cyclic voltammetry (CV) was carried out with a CH Instruments electrochemical analyzer 611C. A three-electrode system consisted of a glassy carbon working electrode, a platinum wire auxiliary electrode, and a 0.1 M Ag/Ag^+ reference electrode. All CV data were recorded with the scan rate of 0.1 Vs^{-1} in CH_3CN with tetrabutylammonium hexafluorophosphate as the supporting electrolyte. All potential values are reported verse ferrocene/ferrocenium ion. X-band EPR spectrum was recorded on a Bruker

Elexsys E-580 spectrometer. ^{1}H NMR spectra were obtained on a Varian AC 400 spectrometer. Element Analyses of carbon, hydrogen, and nitrogen were obtained with a Heraeus CHN-O-S-Rapid Analyzer.

Preparation of [K-18-crown-6-ether][$(NO)_2$Fe(NC_9H_6-NH)] (1). 8-aminoquinoline (0.072 g, 0.5 mmol), potassium tert-butoxide (0.058 g, 0.5 mmol) and 18-crown-6-ether (0.134 g, 0.5 mmol) loaded in a 20 mL Schlenk tube were dissolved in THF (7 mL). The solution was stirred overnight at ambient temperature under N_2 atmosphere and then the resulting suspension was transferred into the Schlenk flask containing [(TMEDA)Fe$(NO)_2$] (0.116 g, 0.5 mmol) by cannula under positive N_2 pressure. After being stirred for 2 h at ambient temperature, the reaction mixture was filtered through Celite to remove the insoluble solid. Hexane was added slowly to the layer above the THF solution. The flask was tightly sealed and kept in the refrigerator at -20℃ for 3 days. The purple crystals of [K-18-crown-6-ether][$(NO)_2$Fe(NC_9H_6-NH)] (**1**) suitable for single-crystal X-ray diffraction analysis were isolated. (yield 0.202 g, 71.7%). IR ν_{NO}: 1655 m, 1603 s cm^{-1} (THF); 1651 m, 1599 s cm^{-1} (CH_3CN); 1646 m, 1650 s cm^{-1} (KBr). ^{1}H NMR (CD_3CN): δ 7.84 (d), 7.80-7.81 (m), 7.03-6.97 (m), 6.30 (dd), 6.18 (dd) ppm. Absorption spectrum (THF) [λ_{max}, nm (ϵ, M^{-1} cm^{-1})]: 348(9728). Anal. Calcd for $C_{21}H_{31}FeKN_4O_8$: C, 44.85; H, 5.56; N, 9.96. Found: C, 44.29; H, 6.01; N, 9.80.

Preparation of [K-18-crown-6-ether][$(NO)_2$Fe(NC_9H_6-O)] (2). 8-quinoline (0.073 g, 0.5 mmol), potassium tert-butoxide (0.058 g, 0.5 mmol) and 18-crown-6-ether (0.134 g, 0.5 mmol) loaded in a 20 mL Schlenk tube were dissolved in THF (7 mL). The solution was stirred overnight at ambient temperature under N_2 atmosphere and then the resulting suspension was transferred into the Schlenk flask containing [(TMEDA)Fe$(NO)_2$] (0.116 g, 0.5 mmol) by cannula under positive N_2 pressure. After being stirred for 2 h at ambient temperature, the reaction mixture was filtered through Celite to remove the insoluble solid. Hexane was added slowly to the layer above the THF solution. The flask was tightly sealed and kept in the refrigerator at -20℃ for 3 days. The yellow-brown crystals of [K-18-crown-6-ether][$(NO)_2$Fe(NC_9H_6-O)] (**2**) suitable for single-crystal X-ray diffraction analysis were isolated. (yield 0.201 g, 71.5%). IR ν_{NO}: 1674 m, 1619 s cm^{-1} (THF); 1667 m, 1613 s cm^{-1} (CH_3CN); 1671 m, 1613 s cm^{-1} (KBr). ^{1}H NMR (CD_3CN): δ 8.12 (dd), 7.84 (dd), 7.33 (t), 7.17-7.20 (m), 6.74 (dd), 6.65 (dd) ppm. Absorption spectrum (THF) [λ_{max}, nm (ϵ, M^{-1} cm^{-1})]: 341(5262), 420(2376), 558(698). Anal. Calcd for $C_{21}H_{30}FeKN_3O_9$: C, 44.77; H, 5.37; N, 7.46. Found: C, 44.53; H, 5.55; N, 7.57.

Preparation of [K-18-crown-6-ether][$(NO)_2$Fe(NC_9H_6-S)] (3). [(TMEDA)Fe$(NO)_2$] (0.047 g, 0.2 mmol), [K][NC_9H_6-S] (0.039 g, 0.2 mmol) and

18-crown-6-ether (0.053 g, 0.2 mmol) loaded in a 20 mL Schlenk tube were dissolved in THF (7 mL). The solution was stirred overnight at ambient temperature under N_2 atmosphere and then the reaction mixture was filtered through Celite to remove the insoluble solid. Hexane was added slowly to the layer above the THF solution. The flask was tightly sealed and kept in the refrigerator at -20℃ for 3 days. The dark red crystals of [K-18-crown-6-ether][$(NO)_2Fe(NC_9H_6$-S)] (**3**) suitable for single-crystal X-ray diffraction analysis were isolated. (yield 0.093 g, 79.9%). IR ν_{NO} : 1660 m, 1612 s cm^{-1} (THF); 1659 m, 1611 s cm^{-1} (CH_3CN); 1655 m, 1607 s cm^{-1} (KBr). ^1H NMR ($(CD_3)_2SO$): δ 8.39 (d), 8.26 (dd), 7.62-7.65 (m), 7.25-7.29(m), 7.22-7.23 (m) ppm. Absorption spectrum (THF) [λ_{max}, nm (ϵ, M^{-1} cm^{-1})]: 332(6936), 411(5717), 509(3107), 746(407). Anal. Calcd for $C_{21}H_{30}FeKN_3O_8S$: C, 43.53; H, 5.22; N, 7.25. Found: C, 43.17; H, 5.65; N, 7.65.

Preparation of [K-18-crown-6-ether][$(NO)_2Fe(SC_6H_4$-*o*-$NH_2)$] (**4**). [(TMEDA)$Fe(NO)_2$] (0.232 g, 1 mmol), [K][SC_6H_4-*o*-NH_2] (0.163 g, 1 mmol) and 18-crown-6-ether (0.267 g, 1 mmol) loaded in a 20 mL Schlenk tube were dissolved in CH_3CN (5 mL). The solution was stirred overnight at ambient temperature under N_2 atmosphere and then the reaction mixture was filtered through Celite to remove the insoluble solid. 5 mL of hexane and 10 mL of diethyl ether were added to precipitate the green solid [K-18-crown-6-ether][$(NO)_2Fe(SC_6H_4$-*o*-$NH_2)$] (**4**) (0.357 g, yield 65.8%). Diethyl ether was added slowly to the layer above the CH_3CN solution of complex 4 and the flask was tightly sealed and kept in the refrigerator at -20℃ for 2 weeks. The dark green crystals of complex 4 suitable for single-crystal X-ray diffraction analysis were isolated. IR ν_{NO} : 1657 m, 1607 s cm^{-1} (CH_3CN); 1643 m, 1585 s cm^{-1} (KBr). ^1H NMR (CH_3CN): δ 7.30 (s), 6.93 (s), 6.76 (s), 6.60 (s), 4.15 (s) ppm. Absorption spectrum (CH_3CN) [λ_{max}, nm (ϵ, M^{-1} cm^{-1})]: 312(6589), 319(6140), 366(4224), 475(1719), 580(1257), 734(580). Anal. Calcd for $C_{18}H_{30}FeKN_3O_8S$: C, 39.78; H, 5.56; N, 7.73. Found: C, 39.58; H, 5.83; N, 7.65.

Preparation of $[PPh_4]_2[(NO)_2Fe(\mu$-SC_6H_4-*o*-$NH_2)]_2$ (5). The CH_3CN solution (7 mL) containing [(TMEDA)$Fe(NO)_2$] (0.116 g, 0.5 mmol) was added slowly to the 20 mL Schlenk tube containing CH_3CN solution (7 mL) of [PPh_4][SC_6H_4-*o*-NH_2] (0.232 g, 0.5 mmol) by cannula under positive N_2 pressure. After the tube was tightly sealed and stood without stirring at the ambient temperature overnight, the dark green crystals of $[PPh_4]_2[(NO)_2Fe(\mu$-SC_6H_4-*o*-$NH_2)]_2$ (**5**) suitable for single-crystal X-ray diffraction analysis were isolated. (yield 0.212 g, 73.1%). IR : 3410 w, 3291 w cm^{-1} (ν_{NH}), 1647 s, 1606 s cm^{-1} (ν_{NO}) (KBr); 1650 m, 1598 s cm^{-1} (ν_{NO}) (DMSO:THF = 1:1(v/v)). ^1H NMR ($(CD_3)_2SO$): δ 7.18 (d), 7.16 (d), 6.81 (t), 6.65 (t), 5.02 (s) ppm. Absorption spectrum (DMSO) [λ_{max}, nm (ϵ, M^{-1} cm^{-1})]: 308(9640), 322(9422),

372(6539), 583(2148), 814(614). Anal. Calcd for $C_{60}H_{52}Fe_2N_6O_4P_2S_2$: C, 62.19; H, 4.52; N, 7.25. Found: C, 62.16; H, 4.93; N, 7.06.

Preparation of $[(NO)_2Fe(\mu\text{-}SC_6H_4\text{-}o\text{-}NH_2)]_2$ (6). 2-aminothiophenol (0.11 mL, 1mmol) was added to the THF solution of $[Fe(CO)_2(NO)_2]$, freshly prepared from the reaction of $[PPN][Fe(CO)_3(NO)]$ (0.708 g, 1 mmol) and $[NO][BF_4]$ (0.118 g, 1 mmol), and stirred for 24 h under N_2 atmosphere at ambient temperature. The reaction was monitored by FT-IR. The IR spectrum showing the stretching bands at 1807 w, 1779 s, 1751 s cm^{-1} (THF) was assigned to the formation of $[(NO)_2Fe(\mu\text{-}SC_6H_4\text{-}o\text{-}NH_2)]_2$ (**6**). The reaction mixture was filtered through Celite to remove the insoluble solid and then hexane was added to precipitate the dark green solid of complex **6** (yield 0.134 g, 55.9 %). Diffusion of hexane into the THF solution of complex 6 at -15℃ for 2 weeks led to dark green crystals suitable for X-ray crystallography. IR ν_{NO}: 1807 w, 1779 s, 1751 s cm^{-1} (THF), 1808 w, 1782 s, 1755 s cm^{-1} (ν_{NO}) (diethyl ether); 1780 m, 1725 s cm^{-1} (KBr).

Preparation of [cation][$(NO)_2Fe(SC_6H_4\text{-}o\text{-}NH_2)_2$] (7) (cation = K-18-crown-6-ether (7a), [PPh_4] (7b)). Complex 6 (0.240 g, 0.5 mmol) and $[K][SC_6H_4\text{-}o\text{-}NH_2]$ (0.163 g, 1 mmol) were loaded in a 50-mL Schlenk flask and dissolved in 10 mL THF. After the reaction mixture was stirred for 3 h, the reaction mixture was added to the 50-mL Schlenk flask containing 0.264 g (1 mmol) of 18-crown-6-ether (or $[PPh_4][Br]$, 1 mmol, 0.420 g). When the reaction mixture was stirred for 2 h, the reaction solution was monitored by FT-IR. The IR spectrum, ν_{NO} 1737 s, 1694 s cm^{-1} (THF), was assigned to the formation of [K-18-crown-6-ether][$(NO)_2Fe(SC_6H_4\text{-}o\text{-}NH_2)_2$] (**7a**) and $[PPh_4][(NO)_2Fe(NO)_2(SC_6H_4\text{-}o\text{-}NH_2)_2]$ (**7b**). The reaction mixture was filtered through Celite and then hexane was added to precipitate the dark brown solid complex **7a** (yield: 0.510 g, 76.3 %) (or complex **7b** yield: 0.523 g, 74.1 %). Diffusion of hexane into the THF solution of complex **7b** at -15℃ for 2 weeks led to dark brown crystals suitable for X-ray crystallography. Complex **7b** :IR ν_{NO}: 1737 s, 1694 s cm^{-1} (THF); 1740 s, 1699 s cm^{-1} (CH_3CN); 1732 s, 1689 s cm^{-1} (KBr). Absorption spectrum (THF) [λ_{max}, nm (ϵ, M^{-1} cm^{-1})]: 316 (10846), 345 (8387), 512 (2903), 788 (706). Anal. Calcd $C_{36}H_{32}FeN_4O_2PS_2$: C, 61.45; H, 4.58; N, 7.95. Found: C, 61.14; H, 4.55; N, 7.40.

Preparation of $[PPh_4][(NO)_2Fe(\mu\text{-}SC_6H_4\text{-}o\text{-}NH_2)]_2$ (8). Complex **7b** (0.141 g, 0.2 mmol) and $[(TMEDA)Fe(NO)_2]$ (0.046 g, 0.2 mmol) were loaded in a 20-mL Schlenk tube and dissolved in 10 mL THF. After the reaction mixture was stirred for 12 h, the reaction solution was monitored by FT-IR. The IR spectrum, ν_{NO} 1687 s, 1666 s cm^{-1} (THF), was assigned to the formation of $[PPh_4][(NO)_2Fe(\mu\text{-}SC_6H_4\text{-}o\text{-}NH_2)]_2$ (**8**). The reaction mixture was filtered through Celite and then hexane was added to precipitate

the dark green solid of complex **8**. (yield: 0.118 g, 72.2 %). Diffusion of hexane into the THF solution of complex **8** at -15℃ for 2 weeks led to dark green crystals suitable for X-ray crystallography. IR ν_{NO}: 1687 s, 1666 s cm^{-1} (THF); 1684 s, 1670 s cm^{-1} (CH_3CN); 1687 s, 1657 s cm^{-1} (KBr). Absorption spectrum (CH_3CN) [λ_{max}, nm (ϵ, M^{-1} cm^{-1})]: 317 (10009), 363 (7483), 480 (2836), 594(2023), 722 (1131). Anal. Calcd $C_{40}H_{40}Fe2N_6O_5PS_2$: C, 52.76; H, 3.94; N, 10.26. Found: C, 53.06; H, 4.25; N, 10.12.

Reaction of [K-18-crown-6-ether][NC_9H_6-O] and [K-18-crown-6-ether][$(NO)_2Fe(NC_9H_6$-NH)] (1). 8-quinolinol (0.044 g, 0.3 mmol), potassium tert-butoxide (0.035 g, 0.3 mmol) and 18-crown-6-ether (0.08 g, 0.3 mmol) were loaded in 20 mL Schlenk tube and dissolved in 7 mL THF. The reaction mixture was stirred for 18 h and then added to the 20 mL Schlenk tube containing complex 1 (0.113 g, 0.2 mmol) by cannula under positive N_2 pressure. After the reaction solution was stirred for 10 h, the reaction was monitored by FT-IR. The IR spectrum displaying two stretching bands at 1674 s, 1619 s cm^{-1} (THF) was assigned to the formation of complex **2**. The reaction mixture was filtered through Celite to remove the insoluble solid and then hexane was added slowly to the layer above the THF filtrate. The flask was tightly sealed and kept in the refrigerator at -20℃ for 3 days. The yellow-brown crystals of complex **2** were isolated. (yield 0.087 g, 51.6%).

Reaction of [K-18-crown-6-ether][NC_9H_6-S] and [K-18-crown-6-ether][$(NO)_2Fe(NC_9H_6$-NH)] (1) (or [K-18-crown-6-ether][$(NO)_2Fe(NC_9H_6$-O)] (2)). 18-crown-6-ether (0.027 g, 0.1 mmol), [K][NC_9H_6-S] (0.020 g, 0.1 mmol) , and complex **1** (0.056 g, 0.1 mmol) (or complex **2** (0.056 g, 0.1 mmol)) were loaded in 20 mL Schlenk tube and dissolved in 7 mL THF. The reaction mixture was stirred for 12 h and monitored by FT-IR. The IR spectrum displaying two stretching bands at 1660 s, 1612 s cm^{-1} (THF) was assigned to the formation of complex **3**. The reaction mixture was filtered through Celite to remove the insoluble solid and then hexane was added slowly to the layer above the THF filtrate. The flask was tightly sealed and kept in the refrigerator at -20℃ for 3 days. The dark red crystals of complex **3** were isolated. (yield 0.032 g, 55.8%; yield 0.041 g, 70.8%).

Reaction of $[PPh_4]_2[(NO)_2Fe(\mu$-SC_6H_4-*o*-$NH_2)]_2$ (5), $[K][BPh_4]$ and 18-crown-6-ether. Complex **5** (0.232 g, 0.2 mmol), $[K][BPh_4]$ (0.148 g, 0.4 mmol) and 18-crown-6-ether (0.107 g, 0.4 mmol) were loaded in 20 mL Schlenk tube and dissolved in 8 mL CH_3CN-THF solution (1:1 volume ratio). The reaction mixture was stirred for 18 h under the N_2 atmosphere at ambient temperature and then dried under vacuum to afford brown solids. After the brown solids redissolved in 8 mL THF, the resulting brown solution was filtered through Celite to remove the insoluble solid. The filtrate was dried under vacuum and redissolved in 8 mL CH_3CN affording

the brown solution. The brown solution was monitored by FT-IR. The IR spectrum displaying two stretching bands at 1657 s, 1607 s cm^{-1} (CH_3CN) was assigned to the formation of complex **4**. After the diethyl ether was added slowly to the layer above the CH_3CN filtrate, the flask was tightly sealed and kept in the refrigerator at -20℃ for 3 days. The dark brown crystals of complex 4 were isolated.(yield 0.105 g, 48.3%)

Reaction of [K-18-crown-6-ether][$(NO)_2Fe(SC_6H_4$-*o*-$NH_2)$] (4) with [PPh_4][Br]. The CH_3CN solution (10 mL) containing [PPh_4][Br] (0.428 g, 1 mmol) was added slowly to the 50 mL Schlenk flask containing CH_3CN solution (10 mL) of complex **4** (0.543 g, 1 mmol) by cannula under positive N_2 pressure. After the tube was tightly sealed and stood without stirring at the ambient temperature overnight, the dark green crystals of complex **5** identified by two stretching bands at 1647 s, 1606 s cm^{-1} (KBr) of IR spectrum were isolated. (yield 0.369 g, 63.7%).

Reaction of [PPh_4]$_2$[$(NO)_2Fe(\mu$-SC_6H_4-*o*-$NH_2)]_2$ (5) with [Cp_2Fe][PF_6]. 7 mL CH_3CN was added to the 20 mL Schlenk tube loaded with complex **5** (0.232 g, 0.2 mmol) and [Cp_2Fe][PF_6] (0.067 g, 0.2 mmol). After the reaction mixture was stirred for 18 h under the N_2 atmosphere at ambient temperature, the reaction mixture was dried under vacuum and redissolved in 15 mL THF affording the dark green solution. The dark green solution was monitored by FTIR. The IR spectrum showing two stretching bands at 1687 s, 1666 s cm^{-1} (THF) was assigned to the formation of complex **8**. The dark green solution was filtered through Celite to remove [PPh_4][PF_6]. After the green filtrate was concentrated to 5 mL, hexane was added to precipitate the green solid. The green solids were washed with 20 mL diethyl ether twice and dried under vacuum to afford green solid of complex **8** (yield 0.132 g, 80.5%).

Reaction of [PPh_4][$(NO)_2Fe(\mu$-SC_6H_4-*o*-$NH_2)]_2$ (8) with [Cp_2Fe][PF_6]. 7 mL CH_3CN was added to the 20 mL Schlenk tube loaded with complex 8 (0.132 g, 0.16 mmol) and [Cp_2Fe][PF_6] (0.053 g, 0.16 mmol). After the reaction mixture was stirred for 18 h under the N_2 atmosphere at ambient temperature, the reaction mixture was dried under vacuum and redissolved in 15 mL THF affording the dark green solution. The dark green solution was monitored by FT-IR. The IR spectrum showing the stretching bands at 1807 w, 1778 s, 1751 s cm^{-1} (THF) was assigned to the formation of complex **6**. The dark green solution was filtered through Celite to remove [PPh_4][PF_6]. After the green filtrate was concentrated to 5 mL, hexane was added to precipitate the dark green solid. The dark green solid was washed with 20 mL diethyl ether twice and dried under vacuum to afford dark green solid of complex **6** (yield 0.046 g, 59.9%).

Reaction of [$(NO)_2Fe(\mu$-SC_6H_4-*o*-$NH_2)]_2$ (6) with Cp_2Co. Complex **6** (0.096 g, 0.2 mmol) and Cp_2Co (0.039 g, 0.2 mmol) was dissolved in THF and stirred under the N_2 atmosphere at ambient temperature After being stirred for 18 h, the green

precipitates were afforded. The green precipitates were washed with 10 mL THF twice and dried under vacuum affording $[Cp_2Co][(NO)_2Fe(\mu\text{-}SC_6H_4\text{-}o\text{-}NH_2)]_2$, identified by FT-IR spectrum (IR: 1686 s, 1665 s cm^{-1} (ν_{NO}) (DMSO:THF = 1:1(v/v))(yield 0.093 g, 69.5%).

Reaction of $[Cp_2Co][(NO)_2Fe(\mu\text{-}SC_6H_4\text{-}o\text{-}NH_2)]_2$ with Cp_2Co. $[Cp_2Co][(NO)_2Fe(\mu\text{-}SC_6H_4\text{-}o\text{-}NH_2)]_2$ (0.119 g, 0.2 mmol) and Cp_2Co (0.116 g, 0.6 mmol) were dissolved in the 10 mL solution composed of THF and DMSO(v/v = 1:1) and stirred for 6 h under N_2 atmosphere at ambient temperature. The reaction was monitored with FTIR. The IR spectrum (1650 s, 1598 s cm^{-1} (ν_{NO}) (DMSO:THF = 1:1(v/v)) was assigned to the formation of $[Cp_2Co]_2[(NO)_2Fe(\mu\text{-}SC_6H_4\text{-}o\text{-}NH_2)]_2$.

Reaction of $[K\text{-}18\text{-}crown\text{-}6\text{-}ether][(NO)_2Fe(SC_6H_4\text{-}o\text{-}NH_2)_2]$ (7a), $KHBEt_3$, and 18-crown-6-ether . Complex **7a** (0.401 g, 0.6 mmol) and 18-crown-6-ether (0.159 g, 0.6 mmol) were dissolved in THF under nitrogen atomsphere. The 0.6 mL of $KHBEt_3$ THF solution (1M) was injected by syringe drop by drop into the THF solution of 18-crown-6-ether and complex **7a** at 0 ℃. After the reaction solution was stirred for 10 min, the reaction mixture was filtered through Celite to remove the insoluble $[K\text{-}18\text{-}crown\text{-}6\text{-}ether][SC_6H_4\text{-}o\text{-}NH_2]$. The filtrate was concentrated and hexane was added to precipitate the light yellow-brown solid. The IR spectrum of the light yellow-brown solid displays two stretching bands at 1643 m, 1585 s cm^{-1} (KBr) was assigned to the formation of complex **4** (yield 0.219 g, 67.3%).

Reaction of $[PPh_4][(NO)_2Fe(SC_6H_4\text{-}o\text{-}NH_2)_2]$ (7b) with Cp_2Co. 5 mL THF and 5 mL CH_3CN were added to the Schlenk flask containing complex **7b** (0.141 g, 0.2 mmol) and Cp_2Co (0.116 g, 0.6 mmol). After the reaction mixture was stirred for 48 h, the resulting green precipitates were afforded. The green precipitates were washed with 10 mL THF twice and dried under vacuum affording complex **5**, identified by FT-IR spectrum (IR: 1648 s, 1606 s cm^{-1} (ν_{NO})(KBr)) (yield 0.055 g, 47%).

Reaction of $[PPh_4][(NO)_2Fe(SC_6H_4\text{-}o\text{-}NH_2)_2]$ (7b) with $[Cp_2Fe][PF_6]$. 7 mL CH_3CN was added to the 20 mL Schlenk tube loaded with complex **7b** (0.141 g, 0.2 mmol) and $[Cp_2Fe][PF_6]$ (0.066 g, 0.2 mmol). After the reaction mixture was stirred for 24 h under the N_2 atmosphere at ambient temperature, the reaction mixture was dried under vacuum and redissolved in 7 mL THF affording the dark green solution. The dark green solution was monitored by FT-IR. The IR spectrum showing the stretching bands at 1807 w, 1778 s, 1751 s cm^{-1} (THF) was assigned to the formation of complex 6. The dark green solution was filtered through Celite to remove $[PPh_4][PF_6]$. After the green filtrate was concentrated to 5 mL, hexane was added to precipitate the dark green solid. The dark green solid was washed with 20 mL hexane twice and dried under vacuum to afford dark green solid of complex **6** (yield 0.045 g, 93.8%).

Reaction of $[PPh_4]_2[(NO)_2Fe(\mu\text{-}SC_6H_4\text{-}o\text{-}NH_2)]_2$ (5) with $(SC_6H_4\text{-}o\text{-}NH_2)_2$. A THF solution of $(SC_6H_4\text{-}o\text{-}NH_2)_2$ (0.050 g, 0.2 mmol) was transferred to a 20-mL Schlenk tube loaded with complex **5** (0.232 g, 0.2 mmol) by a cannula under positive N_2 pressure at ambient temperature. The reaction was stirred for 24 h under nitrogen at ambient temperature and monitored by FT-IR. The IR spectrum showing two absorption bands at 1739 s, 1694 s cm^{-1} (THF) implicated the formation of complex **7b**. The brown solution was concentrated under a vacuum and hexane was added to precipitate dark brown solid of complex **7b** (yield: 0.231 g, 81.9 %).

Reaction of [K-18-crown-6-ether][$(NO)_2Fe(SC_6H_4\text{-}o\text{-}NH_2)$] (4) with $(SC_6H_4\text{-}o\text{-}NH_2)_2$. The 20 mL Schlenk tube containing $(SC_6H_4\text{-}o\text{-}NH_2)_2$ (0.050 g, 0.2 mmol) and complex **4** (0.109 g, 0.2 mmol) was added with 7 mL THF. The reaction was stirred for 24 h under N_2 atmosphere at ambient temperature and monitored by FT-IR. The IR spectrum showing two absorption bands at 1739 s, 1694 s cm^{-1} (THF) implicated the formation of complex **7a**. The brown solution was filtered through Celite to remove insoluble solid. After the brown filtrate was concentrated to 5 mL, hexane was added to precipitate the dark brown solid of complex **7a** (yield: 0.069 g, 51.8 %).

Reaction of $[PPh_4]_2[(NO)_2Fe(\mu\text{-}SC_6H_4\text{-}o\text{-}NH_2)]_2$ (5) with $[(NO)_2Fe(\mu\text{-}SC_6H_4\text{-}o\text{-}NH_2)]_2$ (6). A THF solution of complex **6** (0.096 g, 0.2 mmol) was transferred to a 20-mL Schlenk tube loaded with complex **5** (0.232 g, 0.2 mmol) by a cannula under positive N_2 pressure at ambient temperature. The reaction was stirred for 24 h under nitrogen at ambient temperature and monitored by FT-IR. The IR spectrum showing two absorption bands at 1684 s, 1668 vs cm^{-1} (THF) implicated the formation of complex **8**. The green solution was filtered through Celite to remove insoluble solid. After the green filtrate was concentrated to 5 mL, hexane was added to precipitate the dark green solid of complex **8** (yield: 0.124 g, 75.4 %).

Crystallography. Crystallographic data and structure refinements parameters of complexes **1**-**6** and **8** are summarized in Supplementary Material (Tables S1-S7). The crystals chosen for X-ray diffraction studies measured 0.45 x 0.35 x 0.19 mm for complex **1**, 0.51 x 0.46 x 0.35 mm for complex **2**, 0.60 x 0.12 x 0.05 mm for complex **3**, 0.21 x 0.15 x 0.11 mm for complex **4**, 0.25 x 0.20 x 0.10 mm for complex **5**, 0.20 x 0.11 x 0.05 mm for complexes **6** and 0.25 × 0.25 × 0.14 mm for complex **8**, respectively. Each crystal was mounted on a glass fiber and quickly coated in epoxy resin. Unit-cell parameters were obtained by least-squares refinement. Diffraction measurements for complexes **1**-6 and **8** were carried out on a Nonius Kappa or SMART Apex CCD diffractometer using raphite-monochromated Mo K_α radiation (λ = 0.7107 Å) and between 1.88 and 25.16° for complex **1**, between 1.65 and 25.03° for complex **2**, between 1.58 and 25.00° for complex **3**, between 1.73 and 25.06° for

complex **4**, between 1.71 and 25.00° for complex **5**, 2.42 and 25.03° for complex **6**, between 1.71 and 27.50° for complex **8**. Least-squares refinement of the positional and anisotropic thermal parameters for the contribution of all non-hydrogen atoms and fixed hydrogen atoms was based on F^2. A SADABS absorption correction was made. The SHELXTL structure refinement program was employed.

Captions of Figures

Figure 1. The Fe K-edge absorption spectrum of $[PPh_4]_2[(NO)_2Fe(\mu\text{-}SC_6H_4\text{-}o\text{-}NH_2)]_2$ (**5**).

Figure 2. ORTEP drawing and labeling scheme of $[K\text{-}18\text{-}crown\text{-}6\text{-}ether][(NO)_2Fe(NC_9H_6\text{-}NH)]$ (**1**) with thermal ellipsoids drawn at 30% probability. Selected bond distances (Å) and angles (deg): Fe(1)−N(1), 1.632(9); Fe(1)−N(2), 1.612(10); Fe(1)−N(3), 2.043(13); Fe(1)−N(4), 2.053(15); N(1)−O(1), 1.183(11); N(2)−O(2), 1.183(13); Fe(1)−N(1)−O(1), 168.1(10); Fe(1)−N(2)−O(2), 169.5(9); N(1)−Fe(1)−N(2), 113.2(5); N(3)−Fe(1)−N(4), 77.2(6).

Figure 3. ORTEP drawing and labeling scheme of $[K\text{-}18\text{-}crown\text{-}6\text{-}ether][(NO)_2Fe(NC_9H_6\text{-}O)]$ (**2**) with thermal ellipsoids drawn at 30% probability. Selected bond distances (Å) and angles (deg): Fe(1)−N(1), 1.639(11); Fe(1)−N(2), 1.600(11); Fe(1)−N(3), 2.045(7); Fe(1)−O(3), 2.021(7); N(1)−O(1), 1.215(12); N(2)−O(2), 1.246(13); Fe(1)−N(1)−O(1), 170.4(9); Fe(1)−N(2)−O(2), 169.0(7); N(1)−Fe(1)−N(2), 114.4(4); N(3)−Fe(1)−O(3), 79.1(3).

Figure 4. ORTEP drawing and labeling scheme of $[K\text{-}18\text{-}crown\text{-}6\text{-}ether][(NO)_2Fe(NC_9H_6\text{-}S)]\cdot 2THF$ (**3**) with thermal ellipsoids drawn at 30% probability. Selected bond distances (Å) and angles (deg): Fe−N(1), 1.642(3); Fe−N(2), 1.662(3); Fe−N(3), 2.067(2); Fe−S(1), 2.3162(9); N(1)−O(1), 1.212(3); N(2)−O(2), 1.206(3); Fe−N(1)−O(1), 168.3(2); Fe−N(2)−O(2), 172.1(2); N(1)−Fe−N(2), 117.56(12); N(3)−Fe−S(1), 83.11(7).

Figure 5. ORTEP drawing and labeling scheme of $[K\text{-}18\text{-}crown\text{-}6\text{-}ether][(NO)_2Fe(SC_6H_4\text{-}o\text{-}NH_2)]$ (**4**) with thermal ellipsoids drawn at 50% probability. Selected bond distances (Å) and angles (deg): Fe(1)−N(1), 1.643(6); Fe(1)−N(2), 1.651(5); Fe(1)−N(3), 2.085(5); Fe(1)−S(1), 2.3265(18); N(1)−O(1), 1.207(7); N(2)−O(2), 1.193(6); Fe(1)−N(1)−O(1), 168.8(5); Fe(1)−N(2)−O(2), 168.3(5); N(1)−Fe(1)−N(2), 116.2(3); N(3)−Fe(1)−S(1), 84.27(14).

Figure 6. ORTEP drawing and labeling scheme of $[(NO)_2Fe(\mu\text{-}SC_6H_4\text{-}o\text{-}NH_2)]_2^{2-}$ (**5**) with thermal ellipsoids drawn at 50% probability. Selected bond distances (Å) and angles (deg): Fe···FeA, 3.6408(15); Fe−N(1), 1.668(5); Fe−N(2), 1.660(5); N(1)−O(1), 1.185(7); N(2)−O(2), 1.186(7); Fe−S(1), 2.3855(18); Fe−S(1A), 2.3754(16); Fe−N(1)−O(1), 166.5(5); Fe−N(2)−O(2), 167.5(5); N(1)−Fe−N(2), 114.3(3); N(1)−Fe−S(1), 111.34(18); N(1)−Fe−S(1A), 113.04(18); N(2)−Fe−S(1), 117.9(2); N(2)−Fe−S(1A), 115.75(18); S(1)−Fe−S(1A), 80.24(6).

Figure 7. ORTEP drawing and labeling scheme of $[(NO)_2Fe(\mu\text{-}SC_6H_4\text{-}o\text{-}NH_2)]_2^{-}$ (**8**) with thermal ellipsoids drawn at 50% probability. Selected bond distances (Å) and angles (deg): Fe(1)···Fe(2) 2.9258(5); Fe(1)−N(1), 1.663(2); Fe(1)−N(2), 1.657(2); Fe(2)−N(3), 1.659(2); Fe(2)−N(4), 1.667(2); N(1)−O(1), 1.191(3); N(2)−O(2), 1.179(2); N(3)−O(3), 1.177(3); N(4)−O(4), 1.179(2); Fe(1)−S(1), 2.3003(7); Fe(1)−S(2), 2.3244(7); Fe(2)−S(1), 2.3150(7); Fe(2)−S(2), 2.3114(7); Fe(1)−N(1)−O(1), 167.7(2); Fe(1)−N(2)−O(2), 174.1(2); Fe(2)−N(3)−O(3), 168.7(2); Fe(2)−N(4)−O(4), 170.0(2); N(1)−Fe(1)−N(2), 117.77(11); N(3)−Fe(2)−N(4), 117.16(11); Fe(1)−S(1)−Fe(2), 78.68(2); Fe(1)−S(2)−Fe(2), 78.27(2).

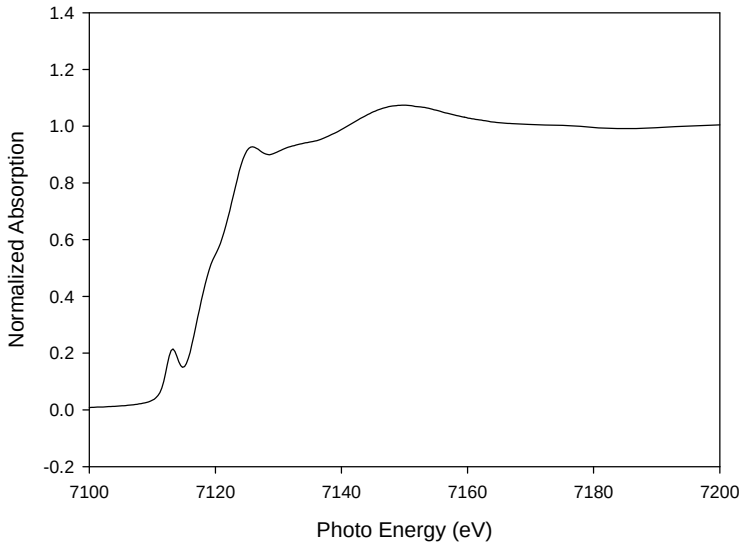

Figure 1

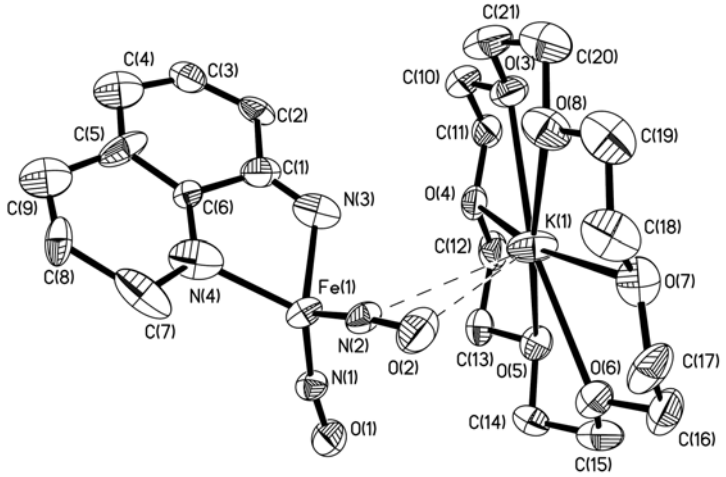

Figure 2

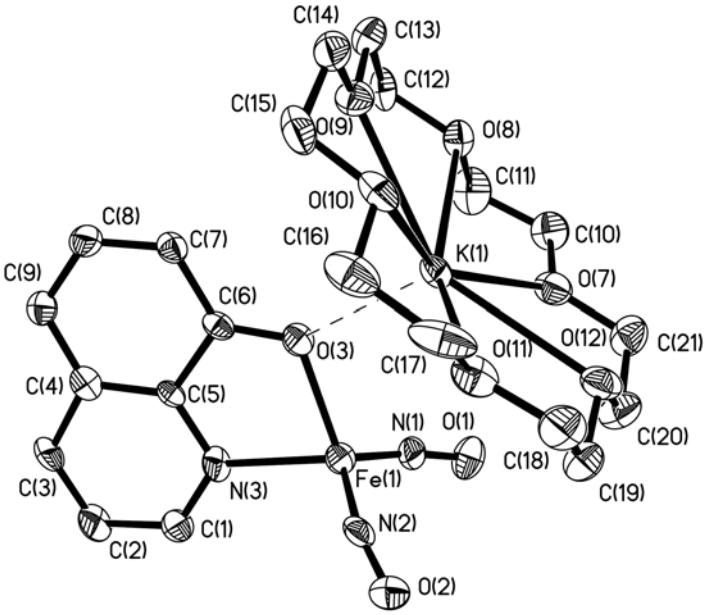

Figure 3

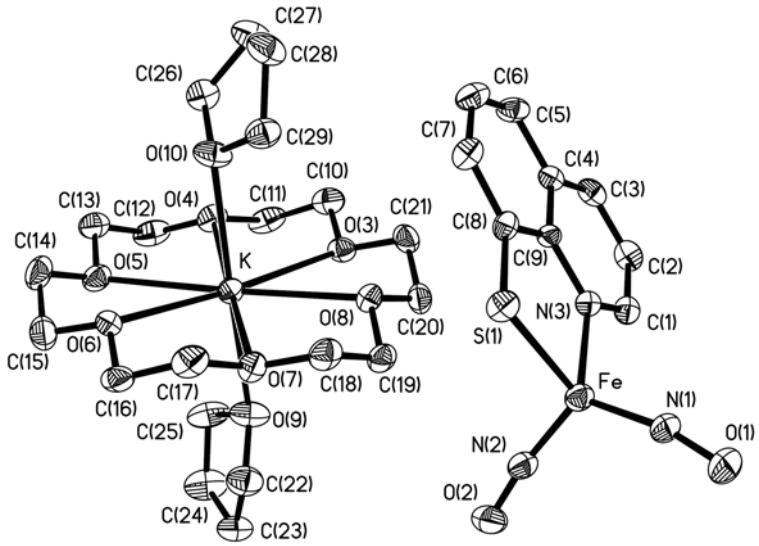

Figure 4

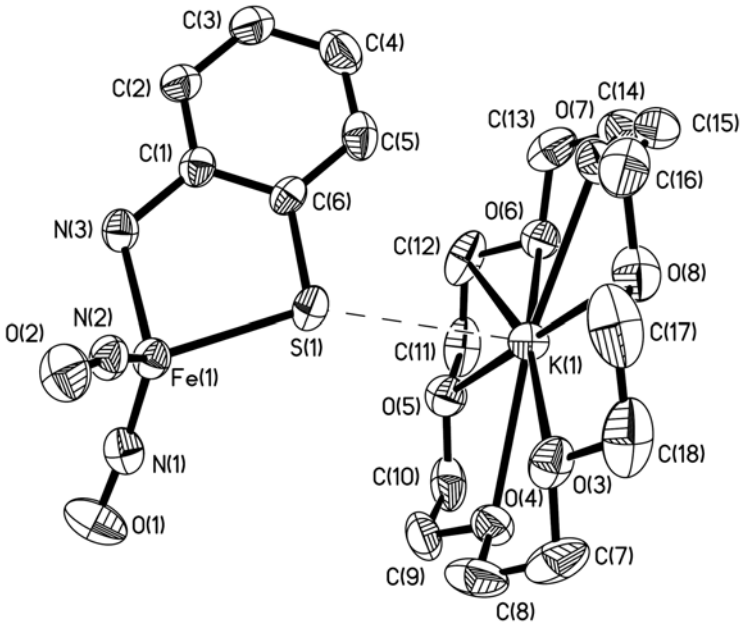

Figure 5

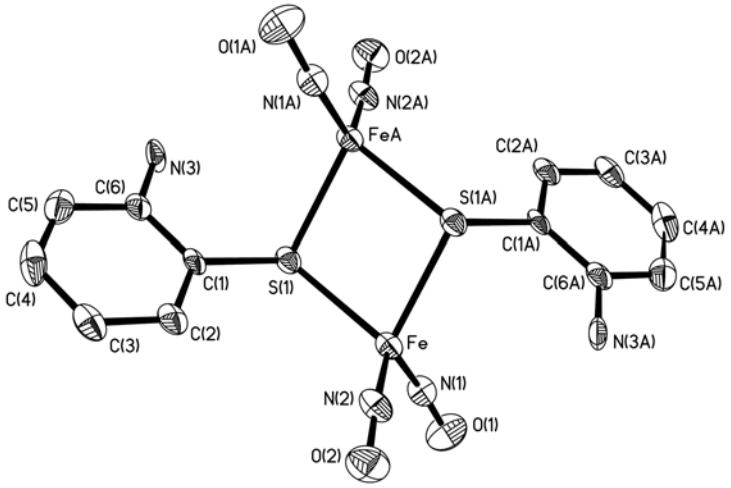

Figure 6

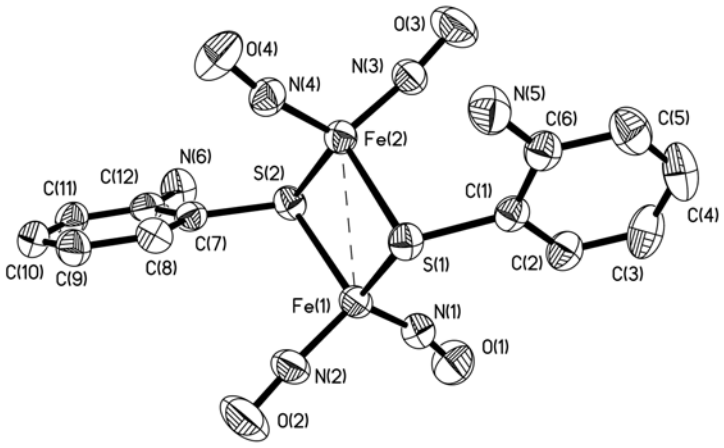

Figure 7

Table 1. Selected Metric Data for Complexes **5**, **6**, and **8**. Dianionic Roussin's Red Ester, Anionic Roussin's Red Ester, and Neutral Roussin's Red Ester.

	5 $\{Fe(NO)_2\}^{10}-\{Fe(NO)_2\}^{10}$	**8** $\{Fe(NO)_2\}^{9}-\{Fe(NO)_2\}^{10}$	**6** $\{Fe(NO)_2\}^{9}-\{Fe(NO)_2\}^{9}$
Fe···Fe (Å)	3.6408(15)	2.9258(5)	2.7065(14)
Fe−N(O) (Å)[a]	1.664(5)	1.662(2)	1.673(5)
N−O (Å)[a]	1.186(7)	1.182(3)	1.160(6)
Fe−S (Å)[a]	2.3805(18)	2.3128(7)	2.2729(15)

Fe−S−Fe ∠(deg)	99.76(6)	78.48(2)	73.08(5)
S−Fe−S ∠(deg)	80.24(6)	101.44(3)	106.92(5)
N−Fe−N ∠(deg)[a]	114.3(3)	117.47(11)	118.2(2)
Fe−N−O ∠(deg)[a]	167.0(5)	170.1(2)	171.0(4)
Dihedral ∠(deg)[b]	180	175.86(21)	180

[a] Average bond distance and angle. [b] Defined by the intersection of two [Fe_2S]

1. (a) Ignarro, L. J., *Nitric oxide: biology and pathobiology*. 2000; (b) Gow, A. J.; Ischiropoulos, H., *J. Cell. Physiol.* **2001,** *187* (3), 277-282.
2. (a) MacMicking, J.; Xie, Q. W.; Nathan, C., *Annu. Rev. Immunol.* **1997,** *15*, 323-350; (b) Bogdan, C., *Nat. Immunol.* **2001,** *2* (10), 907-916.
3. (a) Brenman, J. E.; Bredt, D. S., *Nitric Oxide, Pt B* **1996,** *269*, 119-129; (b) Prast, H.; Philippu, A., *Prog. Neurobiol.* **2001,** *64* (1), 51-68.
4. Ignarro, L. J., *Annu. Rev. Pharmacool. Toxicol.* **1990,** *30*, 535-560.
5. Hussain, S. P.; Trivers, G. E.; Hofseth, L. J.; He, P. J.; Shaikh, I.; Mechanic, L. E.; Doja, S.; Jiang, W. D.; Subleski, J.; Shorts, L.; Haines, D.; Laubach, V. E.; Wiltrout, R. H.; Djurickovic, D.; Harris, C. C., *Cancer Res.* **2004,** *64* (19), 6849-6853.
6. Ueno, T.; Suzuki, Y.; Fujii, S.; Vanin, A. F.; Yoshimura, T., *Biochem. Pharmacol.* **2002,** *63* (3), 485-493.
7. (a) Vanin, A. F., *Nitric Oxide-Biology and Chemistry* **2009,** *21* (1), 1-13; (b) Tsai, M.-L.; Hsieh, C.-H.; Liaw, W.-F., *Inorg. Chem.* **2007,** *46* (12), 5110-5117; (c) Hickok, J. R.; Sahni, S.; Shen, H.; Arvind, A.; Antoniou, C.; Fung, L. W. M.; Thomas, D. D., *Free Radical Biol. Med.* **2011,** *51*, 1558; (d) Rahmanto, Y. S.; Kalinowski, D. S.; Lane, D. J. R.; Lok, H. C.; Richardson, V.; Richardson, D. R., *J. Biol. Chem.* **2012,** *287*, 6960.
8. (a) Foster, M. W.; Cowan, J. A., *J. Am. Chem. Soc.* **1999,** *121* (17), 4093-4100; (b) Cooper, C. E., *Biochim. Biophys. Acta-Bioenerg.* **1999,** *1411* (2-3), 290-309; (c) Wiegant, F. A. C.; Malyshev, I. Y.; Kleschyov, A. L.; Van Faassend, E.; Vanin, A. F., *FEBS Lett.* **1999,** *455* (1,2), 179-182; (d) Boese, M.; Mordvintcev, P. I.; Vanin, A. F.; Busse, R.; Mulsch, A., *J. Biol. Chem.* **1995,** *270* (49), 29244-29249; (e) Mulsch, A.; Mordvintcev, P.; Vanin, A. F.; Busse, R., *FEBS Lett.* **1991,** *294* (3), 252-256; (f) Henry, Y.; Lepoivre, M.; Drapier, J. C.; Ducrocq, C.; Boucher, J. L.; Guissani, A., *FASEB J.* **1993,** *7* (12), 1124-1134; (g) Vithayathil, A. J.; Ternberg, J. L.; Commoner, B., *Nature (London, United Kingdom)* **1965,** *207* (5003), 1246-9.

9. (a) Butler, A. R.; Glidewell, C.; Hyde, A. R.; McGinnis, J.; Seymour, J. E., *Polyhedron* **1983,** *2* (10), 1045-1052; (b) Kennedy, M. C.; Antholine, W. E.; Beinert, H., *J. Biol. Chem.* **1997,** *272* (33), 20340-20347.
10. (a) Tinberg, C. E.; Tonzetich, Z. J.; Wang, H.; Do, L. H.; Yoda, Y.; Cramer, S. P.; Lippard, S. J., *J. Am. Chem. Soc.* **2010,** *132* (51), 18168-18176; (b) Harrop, T. C.; Tonzetich, Z. J.; Reisner, E.; Lippard, S. J., *J. Am. Chem. Soc.* **2008,** *130* (46), 15602-15610.
11. Crack, J. C.; Smith, L. J.; Stapleton, M. R.; Peck, J.; Watmough, N. J.; Buttner, M. J.; Buxton, R. S.; Green, J.; Oganesyan, V. S.; Thomson, A. J.; Le Brun, N. E., *J. Am. Chem. Soc.* **2011,** *133* (4), 1112-1121.
12. (a) Cruz-Ramos, H.; Crack, J.; Wu, G. G.; Hughes, M. N.; Scott, C.; Thomson, A. J.; Green, J.; Poole, R. K., *EMBO J.* **2002,** *21* (13), 3235-3244; (b) Ding, H. G.; Demple, B., *Proc. Natl. Acad. Sci. U. S. A.* **2000,** *97* (10), 5146-5150.
13. (a) Butler, A. R.; Megson, I. L., *Chem. Rev.* **2002,** *102* (4), 1155-1165; (b) Szacilowski, K.; Chmura, A.; Stasicka, Z., *Coord. Chem. Rev.* **2005,** *249* (21-22), 2408-2436; (c) Boese, M.; Keese, M. A.; Becker, K.; Busse, R.; Mulsch, A., *J. Biol. Chem.* **1997,** *272* (35), 21767-21773; (d) Lee, M. H.; Arosio, P.; Cozzi, A.; Chasteen, N. D., *Biochemistry* **1994,** *33* (12), 3679-3687; (e) Tsai, M.-C.; Tsai, F.-T.; Lu, T.-T.; Tsai, M.-L.; Wei, Y.-C.; Hsu, I. J.; Lee, J.-F.; Liaw, W.-F., *Inorg. Chem.* **2009,** *48* (19), 9579-9591; (f) Tonzetich, Z. J.; Wang, H.; Mitra, D.; Tinberg, C. E.; Do, L. H.; Jenney, F. E., Jr.; Adams, M. W. W.; Cramer, S. P.; Lippard, S. J., *J. Am. Chem. Soc.* **2010,** *132* (20), 6914-+.
14. (a) Cesareo, E.; Parker, L. J.; Pedersen, J. Z.; Nuccetelli, M.; Mazzetti, A. P.; Pastore, A.; Federici, G.; Caccuri, A. M.; Ricci, G.; Adams, J. J.; Parker, M. W.; Lo Bello, M., *J. Biol. Chem.* **2005,** *280* (51), 42172-42180; (b) D'Autreaux, B.; Horner, O.; Oddou, J. L.; Jeandey, C.; Gambarelli, S.; Berthomieu, C.; Latour, J. M.; Michaud-Soret, I., *J. Am. Chem. Soc.* **2004,** *126* (19), 6005-6016; (c) Woolum, J. C.; Tiezzi, E.; Commoner, B., *Biochim. Biophys. Acta* **1968,** *160* (3), 311-&.
15. Enemark, J. H.; Feltham, R. D., *Coord. Chem. Rev.* **1974,** *13* (4), 339-406.
16. (a) Chiang, C. Y.; Miller, M. L.; Reibenspies, J. H.; Darensbourg, M. Y., *J. Am. Chem. Soc.* **2004,** *126* (35), 10867-10874; (b) Hsieh, C. H.; Brothers, S. M.; Reibenspies, J. H.; Hall, M. B.; Popescu, C. V.; Darensbourg, M. Y., *Inorg. Chem.* **2013,** *52* (4), 2119-2124; (c) Tonzetich, Z. J.; Do, L. H.; Lippard, S. J., *J. Am. Chem. Soc.* **2009,** *131* (23), 7964-+; (d) Baltusis, L. M.; Karlin, K. D.; Rabinowitz, H. N.; Dewan, J. C.; Lippard, S. J., *Inorg. Chem.* **1980,** *19* (9), 2627-2632; (e) Hung, M.-C.; Tsai, M.-C.; Lee, G.-H.; Liaw, W.-F., *Inorg. Chem.* **2006,** *45* (15), 6041-6047; (f) Huang, H.-W.; Tsou, C.-C.; Kuo, T.-S.; Liaw, W.-F., *Inorg. Chem.* **2008,** *47* (6), 2196-2204.

17. (a) Brockway, L. O.; Anderson, J. S., *Transactions of the Faraday Society* **1937,** *33* (2), 1233-1238; (b) Hedberg, L.; Hedberg, K.; Satija, S. K.; Swanson, B. I., *Inorg. Chem.* **1985,** *24* (18), 2766-2771; (c) Albano, V. G.; Araneo, A.; Bellon, P. L.; Ciani, G.; Manasser.M, *J. Organomet. Chem.* **1974,** *67* (3), 413-422; (d) Wang, R.; Camacho-Fernandez, M. A.; Xu, W.; Zhang, J.; Li, L., *DTr* **2009,** (5), 777-786; (e) Reginato, N.; McCrory, C. T. C.; Pervitsky, D.; Li, L. J., *J. Am. Chem. Soc.* **1999,** *121* (43), 10217-10218; (f) Dillinger, S. A. T.; Schmalle, H. W.; Fox, T.; Berke, H., *DTr* **2007,** (32), 3562-3571.

18. (a) Yeh, S.-W.; Lin, C.-W.; Li, Y.-W.; Hsu, I. J.; Chen, C.-H.; Jang, L.-Y.; Lee, J.-F.; Liaw, W.-F., *Inorg. Chem.* **2012,** *51* (7), 4076-4087; (b) Wang, J.-H.; Chen, C.-H., *Inorg. Chem.* **2010,** *49* (17), 7644-7646; (c) Chen, C.-H.; Chiou, S.-J.; Chen, H.-Y., *Inorg. Chem.* **2010,** *49* (5), 2023-2025.

19. (a) Tsai, F. T.; Chiou, S. J.; Tsai, M. C.; Huang, H. W.; Chiang, M. H.; Liaw, W. F., *Inorg. Chem.* **2005,** *44* (16), 5872-5881; (b) Tonzetich, Z. J.; Heroguel, F.; Do, L. H.; Lippard, S. J., *Inorg. Chem.* **2011,** *50* (4), 1570-1579.

20. (a) Tsou, C.-C.; Lu, T.-T.; Liaw, W.-F., *J. Am. Chem. Soc.* **2007,** *129* (42), 12626-+; (b) Lu, T.-T.; Tsou, C.-C.; Huang, H.-W.; Hsu, I. J.; Chen, J.-M.; Kuo, T.-S.; Wang, Y.; Liaw, W.-F., *Inorg. Chem.* **2008,** *47* (13), 6040-6050.

21. (a) Jo, D.-H.; Chiou, Y.-M.; Que, L., *Inorg. Chem.* **2001,** *40* (13), 3181-3190; (b) Chen, C.-H.; Ho, Y.-C.; Lee, G.-H., *J. Organomet. Chem.* **2009,** *694* (21), 3395-3400; (c) Tsai, F. T.; Lee, Y. C.; Chiang, M. H.; Liaw, W. F., *Inorg. Chem.* **2013,** *52* (1), 464-473; (d) Tsai, F.-T.; Kuo, T.-S.; Liaw, W.-F., *J. Am. Chem. Soc.* **2009,** *131* (10), 3426-3427; (e) Shih, W. C.; Lu, T. T.; Yang, L. B.; Tsai, F. T.; Chiang, M. H.; Lee, J. F.; Chiang, Y. W.; Liaw, W. F., *J. Inorg. Biochem.* **2012,** *113*, 83-93.

22. Tsai, M.-L.; Liaw, W.-F., *Inorg. Chem.* **2006,** *45* (17), 6583-6585.

23. Lu, T.-T.; Lai, S.-H.; Li, Y.-W.; Hsu, I. J.; Jang, L.-Y.; Lee, J.-F.; Chen, I. C.; Liaw, W.-F., *Inorg. Chem.* **2011,** *50* (12), 5396-5406.

24. (a) Lu, T.-T.; Chiou, S.-J.; Chen, C.-Y.; Liaw, W.-F., *Inorg. Chem.* **2006,** *45* (21), 8799-8806; (b) Tsou, C. C.; Tsai, F. T.; Chen, H. Y.; Hsu, I. J.; Liaw, W. F., *Inorg. Chem.* **2013,** *52* (3), 1631-1639.

25. Chong, K. S.; Rettig, S. J.; Storr, A.; Trotter, J., *Canadian Journal of Chemistry-Revue Canadienne De Chimie* **1979,** *57* (23), 3099-3106.

26. McBride, D. W.; Stafford, S. L.; Stone, F. G. A., *Inorg. Chem.* **1962,** *1* (2), 386-388.

國科會補助計畫衍生研發成果推廣資料表

日期:2014/02/26

國科會補助計畫	計畫名稱: 新穎?亞硝醯基鐵化合物之合成、結構、反應性及其電子結構之探討
	計畫主持人: 陳建宏
	計畫編號: 100-2113-M-040-004-MY2　　學門領域: 生物無機化學

無研發成果推廣資料

100 年度專題研究計畫研究成果彙整表

計畫主持人：陳建宏	計畫編號：100-2113-M-040-004-MY2
計畫名稱：新穎?亞硝醯基鐵化合物之合成、結構、反應性及其電子結構之探討	

成果項目			量化			單位	備註（質化說明：如數個計畫共同成果、成果列為該期刊之封面故事...等）
			實際已達成數（被接受或已發表）	預期總達成數(含實際已達成數)	本計畫實際貢獻百分比		
國內	論文著作	期刊論文	0	0	100%	篇	
		研究報告/技術報告	0	0	100%		
		研討會論文	0	0	100%		
		專書	0	0	100%		
	專利	申請中件數	0	0	100%	件	
		已獲得件數	0	0	100%		
	技術移轉	件數	0	0	100%	件	
		權利金	0	0	100%	千元	
	參與計畫人力（本國籍）	碩士生	2	2	100%	人次	
		博士生	0	0	100%		
		博士後研究員	0	0	100%		
		專任助理	0	0	100%		
國外	論文著作	期刊論文	0	0	100%	篇	
		研究報告/技術報告	0	0	100%		
		研討會論文	0	0	100%		
		專書	0	0	100%	章/本	
	專利	申請中件數	0	0	100%	件	
		已獲得件數	0	0	100%		
	技術移轉	件數	0	0	100%	件	
		權利金	0	0	100%	千元	
	參與計畫人力（外國籍）	碩士生	0	0	100%	人次	
		博士生	0	0	100%		
		博士後研究員	0	0	100%		
		專任助理	0	0	100%		

其他成果 (無法以量化表達之成果如辦理學術活動、獲得獎項、重要國際合作、研究成果國際影響力及其他協助產業技術發展之具體效益事項等，請以文字敘述填列。)	無

	成果項目	量化	名稱或內容性質簡述
科教處計畫加填項目	測驗工具(含質性與量性)	0	
	課程/模組	0	
	電腦及網路系統或工具	0	
	教材	0	
	舉辦之活動/競賽	0	
	研討會/工作坊	0	
	電子報、網站	0	
	計畫成果推廣之參與（閱聽）人數	0	

國科會補助專題研究計畫成果報告自評表

請就研究內容與原計畫相符程度、達成預期目標情況、研究成果之學術或應用價值（簡要敘述成果所代表之意義、價值、影響或進一步發展之可能性）、是否適合在學術期刊發表或申請專利、主要發現或其他有關價值等，作一綜合評估。

1. 請就研究內容與原計畫相符程度、達成預期目標情況作一綜合評估 ■達成目標 □未達成目標（請說明，以 100 字為限） □實驗失敗 □因故實驗中斷 □其他原因 說明：
2. 研究成果在學術期刊發表或申請專利等情形： 論文：□已發表 □未發表之文稿 ■撰寫中 □無 專利：□已獲得 □申請中 ■無 技轉：□已技轉 □洽談中 ■無 其他：(以 100 字為限)
3. 請依學術成就、技術創新、社會影響等方面，評估研究成果之學術或應用價值（簡要敘述成果所代表之意義、價值、影響或進一步發展之可能性）(以 500 字為限)